Extracellular AGR2 triggers lung tumour cell proliferation through repression of p21(CIP1)

Delphine Fessart, Claire de Barbeyrac, Ines Boutin, Thomas Grenier, Elodie Richard, Hughes Begueret, David Bernard, Eric Chevet, Jacques Robert, Frederic Delom

Extracellular AGR2 triggers lung tumour cell proliferation through repression of p21^{CIP1}

Delphine Fessart[1,2,3*], Claire de Barbeyrac[1†], Ines Boutin[1†], Thomas Grenier[1†], Elodie Richard[1], Hughes Begueret[1,4], David Bernard[5], Eric Chevet[2,3], Jacques Robert[1] and Frederic Delom[1*]

[1]ARTiSt Group, Univ. Bordeaux, INSERM, Institut Bergonié, ACTION, U1218, F-33000 Bordeaux, France ; [2]INSERM U1242, "Chemistry, Oncogenesis Stress Signaling", Univ. Rennes, Rennes, France ; [3]Centre de Lutte Contre le Cancer Eugène Marquis, Rennes, France ; [4]Dept of Pathology, University Hospital of Bordeaux, Hopital Haut-Lévêque, Pessac, France; [5]Inserm U1052, CNRS UMR 5286, Université de Lyon & Centre Léon Bérard, Centre de Recherche en Cancérologie de Lyon, Lyon, France.

[†]These authors contributed equally to this work

*Correspondence to: FD - E-mail: frederic.delom@u-bordeaux.fr or DF - E-mail: delphine.fessart@inserm.fr

Abstract

The human Anterior GRadient 2 (AGR2) protein is an Endoplasmic Reticulum (ER)-resident protein which belongs to the Protein-Disulfide Isomerase (PDI) superfamily and is involved to productive protein folding in the ER. As such AGR2, often found overexpressed in adenocarcinomas, contributes to tumour development by enhancing ER proteostasis. We previously demonstrated that AGR2 is secreted (extracellular AGR2 (eAGR2)) in the tumour microenvironment and plays extracellular roles independent of its ER functions. Herein, we show that eAGR2 triggers cell proliferation and characterize the underlying molecular mechanisms. We demonstrate that eAGR2 enhances tumour cell growth by repressing the tumour suppressor p21^{CIP1}. Our findings shed light on a novel mechanism through which eAGR2 behaves as a growth factor in the tumour microenvironment, independently of its ER function, thus promoting tumour cell growth through repression of p21^{CIP1}. Our results provide a rationale for targeting eAGR2/ p21^{CIP1}-based signalling as a potential therapeutic target to impede tumour growth.

Keywords: AGR2; Endoplasmic Reticulum; Lung Cancer, Tumour Microenvironment; p21CIP1.

1. Introduction

Lung cancer is the most common cancer worldwide, killing 1.2 million people annually (World Health Organization, 2009). Of lung cancers diagnosed, over 80% are Non-Small Cell Lung Cancer (NSCLC), comprising adenocarcinoma, squamous cell carcinoma and large cell carcinoma. Because of the lack of biomarkers, the majority of NSCLC patients are usually diagnosed at late stages and succumbs in the absence of efficient treatment. Therefore, the identification of new markers of NSCLC progression is critical for both early cancer detection and for the development of novel therapeutic approaches to treat this dismal cancer. Recently, we demonstrated *in vitro* and *in vivo* that Anterior Gradient 2 (AGR2) expression levels positively correlate with lung cancer progression and aggressiveness [1-5]. As such we propose that AGR2 protein could represent a new biomarker for lung cancer [2].

Human AGR2 is an Endoplasmic Reticulum (ER)-resident protein belonging to the Protein-Disulfide Isomerase (PDI) superfamily (PDIA17) [3]. We first identified AGR2 as part of a complex binding to nascent protein chains at the ER translocon [4]. An increased expression of AGR2 was first described in human breast cancer, followed by many human adenocarcinomas (oesophagus, pancreas, ovary, prostate, etc...) [3]. Recent data showed that AGR2 not only exists as a monomer but can also form homodimers through a motif $E_{60}ALYK_{64}$ [6]. Recently, we demonstrated that the AGR2 monomer/homodimer balance in the ER [6, 7] is important for AGR2 signalling [8] and that intracellular AGR2 (iAGR2) is involved in ER protein folding and quality control [3, 4, 9]. When AGR2 is secreted (extracellular AGR2 (eAGR2)) in the tumour microenvironment, it participates to the preneoplastic phenotype and contributes to epithelial tumorigenicity [2, 3, 8, 9]. Indeed, in our 3D lung organoid/tumoroid models [2, 10, 11], we have demonstrated that eAGR2 in the lung tumour microenvironment is sufficient by itself to induce epithelial morphogenesis disruption and to increase the cancer cell metastasis potential [2]. Similarly, other ER-resident PDI proteins are found secreted in the extracellular microenvironment. For example, we have shown that PDIA2 is secreted into the lumen of the thyroid follicles by thyrocytes to control extracellular thyroglobulin folding and multimerization [12, 13]. It has been also reported that PDIA3 is secreted and interacts with extracellular matrix proteins [14] and that QSOX1 is secreted and participates in laminin assembly thereby controlling extracellular matrix functionality [15]. Moreover, we demonstrated recently that eAGR2 secretion results in chemoattraction of monocytes and inflammatory phenotypes [8].

Cell growth in normal tissue is tightly regulated while lost in tumours. Abnormal growth control is not only operative in early oncogenesis but also during metastasis spreading. Thus, it is crucial to understand how and when this occurs, and then to use this knowledge to identify novel therapeutic targets and subsequent approaches that would more specifically kill tumour cells without damaging normal tissues. We and others have demonstrated a direct link between AGR2 overexpression and tumour cell proliferation increase [1-3]; however, the molecular mechanisms at the origin of this phenotype are not fully understood. Thus, in this work, we investigated the role of AGR2 using exogenous activation and knock-down strategies. We demonstrate that AGR2 has a positive role in tumour growth, and that eAGR2 alone can attenuate *CDKN1A* ($p21^{CIP1}$) expression, thereby favouring tumour growth.

2. Materials and methods

2.1. Cohort

Samples of human lung cancer tissues were obtained from the Haut-Levêque University Hospital (Bordeaux, France) and reviewed by an expert pathologist (H. Begueret). The number of human lung samples analyzed and their clinicopathological characteristics are described in Tables 1 and 2. These procedures were approved by the Institutional Review Board at Haut-Levêque University Hospital (NFS96900). Immediately after the surgical resection, tumour specimens were fixed for 24 hr in 10% buffered formaldehyde, dehydrated and routinely embedded in paraffin. All staining procedures were performed in an automated immunostainer (Bond-III, Leica Biosystems Newcastle Ltd, Newcastle-Upon-Tyne, U.K) as previously described in [2]. For visualization, the Bond Polymer Refine Detection kit (Leica Biosystems Newcastle Ltd, Newcastle-Upon-Tyne, U.K) was used according to the manufacturer's instructions. Sections were visualized with a Leica DMIL LED microscope, and images were acquired using LAS X imaging software (Leica). Quantification was done using ImageJ software and by analyzing 4 fields per sample.

2.2. Cell lines and cell culture

Human normal bronchial epithelial cells (HBEC) and lung cancer cells have been previously described [10]. All cell lines used for this study were mycoplasma-free. All cancer cells were cultured in DMEM supplemented with 10% FBS. ShRNA against AGR2 was described in [2]. In order to overexpress AGR2 or AGR2 constructs (AGR2-C18S and AGR2-E60A), HBECs were infected with an empty vector pLenti6.3/V5 or a pLenti6.3/V5 vector expressing either the coding sequence of human AGR2, or that of the constructs AGR2-C81S and AGR2-E60A. The ShRNA against $p21^{CIP1}$ was previously described [16].

2.3. Antibodies and reagents

The sources of the primary antibodies used in these studies were as follows: polyclonal rabbit anti-human calnexin (Cell Signalling), monoclonal mouse anti-human AGR2 (Abnova, clone 1C3), monoclonal anti-human $p21^{Waf1/Cip1}$ (DCS60) Antibody (Cell Signalling), monoclonal mouse anti-Human p53 Protein (Agilent, Clone DO-7), monoclonal mouse anti-human cyclin

A (B-8) (Santa Cruz), mouse anti-Human Rb (BD Biosciences), monoclonal anti-human GAPDH (Clone 6C5, Millipore), polyclonal rabbit anti-human Akt (Cell signalling), polyclonal rabbit anti-human phospho-Akt (Ser473) (Cell Signalling) and monoclonal mouse anti-human c-Myc (BD Biosciences) and peroxidase-conjugated anti-rabbit and anti-mouse Ig (Amersham) as secondary antibodies. The secondary antibodies used were as follows: Alexa-Fluor-488- and Alexa-Fluor-546-conjugated anti-mouse and rabbit IgGs (Molecular Probes/Invitrogen). Reagents used in the study were diaminophenylindole (DAPI) (Sigma-Aldrich,), paraformaldehyde (Sigma-Aldrich) and MG132 (Sigma-Aldrich).

2.4. Western blot analysis

Cells were seeded in 6-well plates and grown for 3 days. Cells were lysed in RIPA buffer (0.05 M Tris-HCl pH7.4, 0.15 M NaCl, 1% Nonidet P-40, 0.1% deoxycholate, 1 mM $CaCl_2$) containing protease and phosphatase inhibitors. After centrifugation, proteins in the supernatant were quantified, boiled with Laemmli buffer, resolved by SDS-PAGE and transferred to a nitrocellulose membrane as described previously [17]. For proteasome inhibition, cells were incubated for 4 h with 10 µM of MG132 at 37°C before lysis.

2.5. Immunofluorescence

For staining at the plasma membrane, cells were cultured on coverslips for 72 h and incubated with the AGR2 primary antibody for 2 h before fixation. Cells were then fixed using 4% PFA in PBS for 15 min and then, incubated with the secondary antibody (Life Technologies) for 1 hr at RT in PBS with 0.5% Tween 20 and 1% BSA as previously described [18]. DAPI staining was used to visualize the nucleus. Confocal analysis was performed using Nikon confocal imaging system. Images were generated and converted to Tiff format. For the others immunofluorescence staining, cells cultured on coverslips were fixed using 4% PFA in PBS for 15 min and then permeabilized with 0.1% Nonidet P40. Cells were incubated with the primary antibody O/N in PBS-0.5% Tween 20 and 1% BSA. Cells were then washed and incubated with secondary antibodies (Life Technologies) for 1 hr at RT as we previously described [19]. DAPI staining was used to visualize the nucleus. Microscopy analysis was performed using Leica DMi8 imaging system. Images were generated and converted to jpeg format.

2.6. Cell proliferation

Cells were seeded in 96-well format using the Perkin Elmer Janus Mini liquid handling platform. Plates were incubated at the indicated time, and medium was changed every day. Before reading, cells were incubated 30 min with the Readyprobes blue (Invitrogen) for nuclei staining (live-cell imaging) or fixed with paraformaldehyde and stained with DAPI [19]. High-content images were acquired with the Cytation 3 automated microscope (Biotek) at 4× magnification, and analysis was performed using the Analysis software (Biotek).

2.7. Apoptosis assay

Cells were seeded into a 96-well plate and grown for 3 days. Cells were then stained for 30 min with NucBlue Live ReadyProbes Reagent and NucGreen Dead 488 ReadyProbes Reagent (ThermoFisher). The 96-well plate was imaged immediately. High-content images were acquired with the Cytation 3 automated microscope (Biotek) at 4× magnification, and analysis was performed using the Analysis software (Biotek). Cells were imaged in the fluorescein isothiocyanate (FITC) (NucGreen) and 4’,6-diamidino-2-phenylindole (DAPI) (NucBlue) channels. A cell was defined as undergoing apoptosis when 50% or more of the nucleus, as defined by NucBlue-positive pixels, was overlapped by NucGreen-positive pixels. Dithiothreitol (DTT, Sigma) was used as a positive control at a single dose of 5 mM for 24 h.

2.8. Cell cycle analysis

Cells were seeded into 10 cm diameter dishes and grown for 3 days. Cells were collected and fixed and then incubated with RNAse A (Promega). Propidium Iodide Solution (BioLegend) was added followed by 30 min incubation in the dark. Cellular DNA content was analysed by a FACS Calibur (Becton Dickinson). Data were processed using FlowJo Software.

2.9 Reverse transcription (RT)-PCR and real-time quantitative PCR

RNA was extracted using the ReliaPrep Cell and Tissue Miniprep Isolation Kit (Promega). One microgram of total RNA was reverse-transcribed to cDNA by the Superscript III Reverse Transcript Kit (Invitrogen). A two-step RT-PCR was used to analyze mRNA expression of

the p21/CIP1, AGR2, and housekeeping gene GAPDH. We used the following gene-specific primers (*CDKN1A* ($p21^{CIP1}$): TGGAGACTCTCAGGGTCGAAA (F); GGCGTTTGGAGTGGTAGAAATC (R); *GAPDH*: CCTGGTATGACAACGAATTT (F); GTGAGGGTCTCTCTCTTCCT (R); and *AGR2*: ATGAGTGCCCACACAGTCAA (F); GGACATACTGGCCATCAGGA (R)). Real-time PCR was carried out in a 25 μL solution containing cDNA, 2× SYBR Green Mastermix (Applied Biosystems), cDNA synthesis reaction and RNase-free water in presence of primers in a One-Step Plus Real-time PCR system (Applied Biosystems).

2.10. Statistical analyses

All results were evaluated using GraphPad Prism statistical software package. Different statistical tests were used according to the type of data analyzed (Student's t-test, Two-way Anova), as is indicated in figure legends. $p \leq 0.05$ was considered as statistically significant.

3. Results

3.1. AGR2 is expressed in human lungs.

Recently, we have reported that AGR2 expression in Non-Small Cell Lung Cancer (NSCLC) tissues is essentially restricted to type II pneumocytes [2]. Here, we investigated the localization and the expression of AGR2 in the normal lung tree, which is composed of conducting airways (bronchi and bronchioles) as well as gas exchanging airways representing the acini (respiratory bronchioles and alveolar ducts). In the lung tree, AGR2 is expressed both in the conducting airways and in the acini (Fig. 1A).

3.2. AGR2 is upregulated in lung cancer tissues

Previously, we reported that AGR2 expression was altered in lung tumours [2]. Hence, we investigated the expression of AGR2 in a cohort of 90 lung cancers patients (Table 1), including adenocarcinoma and squamous cell lung carcinoma. We evaluated the expression of AGR2 protein in adjacent non-tumour (ANT) and tumour tissue samples at different stages (Fig. 1B). Immunohistochemistry revealed that AGR2 was significantly overexpressed in tumour tissue (T) compared to adjacent non-tumour tissue (ANT) (Fig. 1C), as we reported previously [2]. To validate the portability and consistency of the data concerning tumour and non-tumour AGR2 expression, we explored a lung cohort from TCGA datasets. AGR2 expression was significantly higher in tumour tissue as compared to paired adjacent normal tissue (Fig. 1D, E) in lung adenocarcinomas (LUAD) as well as squamous cell carcinomas (LUSC). Hence, our results demonstrate that AGR2 is overexpressed in lung cancer, suggesting a function for this ER-resident chaperone in bronchial tumours.

3.3. Role of two major functional domains of AGR2 in cell growth.

Recently, we demonstrated that overexpression of AGR2 increases cell proliferation [2]. AGR2 has two major functional domains: a dimerization domain (amino acids 60-64) [20] and a thioredoxin-like domain [2] (amino acids 81-84). To test the relevance of these two AGR2 domains in tumour cell growth, we overexpressed two different AGR2 constructs, AGR2-E60A (mutated dimerization domain [8]) and AGR2-C81S (SXXS, inactive form of AGR2 thioredoxin-like domain [2]) as compared to AGR2 wild-type (WT) (Fig. 2A), in non-

tumourigenic primary Human Bronchial Epithelial cells (HBEC) using lentivirus-mediated infection. Overexpression of these constructs in HBEC was confirmed using Western blot with anti-AGR2 antibodies (Fig. 2B). As previously demonstrated, in HBEC-AGR2-WT cells, AGR2 localized with calnexin (CANX), an ER resident type I integral membrane protein (Fig. 2C, AGR2-WT) [2]. As expected, the two AGR2 variants were localized in the same compartment as AGR2-WT (Fig. 2C, AGR2-E60A and AGR2-C81S). As expected, AGR2-WT overexpression enhanced cell proliferation (Fig. 2D). Remarkably, the overexpression of both AGR2-E60A (Fig. 2E) and AGR2-C81S (Fig. 2F) also promoted cell proliferation similarly to what was observed with AGR2-WT (Fig. 2E-F). These results show that these two functional domains, dimerization (AGR2-E60A) and thioredoxin-like (AGR2-C81S), are not required to promote cell proliferation.

3.4. AGR2 inhibits p21 expression

We previously showed that AGR2 was a positive mediator of cell proliferation [2]. We, therefore, raised the hypothesis that the tumour suppressor CDKN1A ($p21^{CIP1}$) might be a potential intermediate in tumour cell proliferation induced by AGR2 [3]. First, we monitored the possible correlation between AGR2 and $p21^{CIP1}$ expression in a panel of human lung epithelial cell lines. High AGR2 expression was only observed in lung tumour cell lines (A549, H460, H23, H1838) compared to the non-tumourigenic HBEC (Fig. 3A). In contrast, high $p21^{CIP1}$ expression was only observed in HBEC (Fig. 3A). To further document the inverse correlation between AGR2 and $p21^{CIP1}$ expression levels observed in cell lines, we evaluated the expression of $p21^{CIP1}$ in HBEC and HBEC-AGR2-WT cells using Western blotting (Fig. 3B). Consistent with the data presented in Fig. 3A, AGR2 overexpression correlated with low $p21^{CIP1}$ protein expression (Fig. 3B and C). In contrast, in lung cancer cells depleted for AGR2 (A549-Sh-AGR2), AGR2 depletion was correlated with increased $p21^{CIP1}$ protein expression compared to A549-Sh-Ctl cells, which endogenously overexpressed AGR2 (Fig. 3D and E).

3.5. Downregulation of $p21^{CIP1}$ reverses the inhibition of tumour cell growth induced by AGR2 knockdown.

As we reported previously, tumour cell proliferation is strongly inhibited in lung

cancer cells depleted for AGR2 and is independent of cell death [2]. To assess the requirement for $p21^{CIP1}$ in the tumour cell growth inhibition induced by AGR2 depletion, we silenced $p21^{CIP1}$, in A549 and A549-AGR2 depleted (A549-Sh-AGR2) cells, using lentivirus-mediated infection with p21 ShRNA. First, we controlled the efficacy of $p21^{CIP1}$ depletion using Western blotting in A549-Sh-p21 and 4549-Sh-AGR2-Sh-p21 (Fig. 4A-C). Then, we measured the impact of $p21^{CIP1}$ depletion on cell growth of A549 (A549-Sh-p21) and A549-AGR2 depleted cells (4549-Sh-AGR2-Sh-p21) (Fig. 4D). A549-Sh-p21 (p21 depletion) cells exhibited a similar proliferation as A549-Sh-Ctl cells. Remarkably, $p21^{CIP1}$ depletion in A549-AGR2 depleted cells (A549-Sh-AGR2-Sh-p21) reversed significantly tumour cell proliferation inhibition induced by AGR2 depletion (A549-Sh-AGR2) (Fig. 4D). Flow cytometry analysis showed that $p21^{CIP1}$ depletion (A549-Sh-p21) did not modify the cell cycle distribution in our experimental conditions (Fig. 4E). In contrast, AGR2 depletion (A549-Sh-AGR2), driving tumour cell growth inhibition (Fig. 4D), showed an increased proportion of cells on G1-phase (Fig. 4E) without any impact on apoptosis (Fig. 4F). These results rule out any apoptotic/survival effects that would explain the different variations observed on cell proliferation. Flow cytometry analysis showed, also, that the depletion of $p21^{CIP1}$ in A549-AGR2 depleted cells (A549-Sh-AGR2-Sh-p21), which reversed significantly the tumour cell growth inhibition induced by AGR2 depletion (A549-Sh-AGR2) (Fig. 4D), was also abrogating the increased proportion of cells in the G1-phase and the decrease proportion of cells in G2/M phase (Fig. 4E). Together, these results demonstrate that $p21^{CIP1}$ plays a crucial role in AGR2-mediated lung cancer cell proliferation.

3.6. Altered AGR2 expression affects $p21^{CIP1}$ cell cycle kinases.

To further document how AGR2 affected the cell cycle, we analyzed the cell cycle of HBEC-AGR2 as compared to that of HBEC using flow cytometry (Figure 4G). We showed that overexpression of AGR2 (HBEC-AGR2) induced an increase of the cell population in the G2-M phase (Fig. 4G). We next evaluated the expression of Rb and cyclin A in HBEC as compared to HBEC-AGR2 cells using Western blotting (Fig. 4H, I) to determine how AGR2 affects the $p21^{CIP1}$ cell cycle kinase targets. It has been demonstrated that p21 positively regulates the expression of Rb [21] and negatively that of cyclin A [21]. AGR2 overexpression, which correlates with a decrease in $p21^{CIP1}$ protein expression (Fig. 3B and C), correlated with low Rb and high cyclin A protein expression (Fig. 4H, I). These results

demonstrated that AGR2 regulates, via the $p21^{CIP1}$ protein, the $p21^{CIP1}$-dependent cell cycle pathway.

3.7. AGR2 inhibits $p21^{CIP1}$ expression in a p53-independent manner.

It has been reported that AGR2 might regulate p53 expression [3, 22]. $p21^{CIP1}$ is an important p53 downstream target gene, and it plays a key role in p53-mediated cell growth arrest and cell apoptosis [23]. Hence, to investigate whether AGR2 could induce p21 inhibition in a p53-dependent manner, we compared HBEC and HBEC overexpressing AGR2 (HBEC-AGR2) treated with ctl and p53 siRNAs. Seventy-two hours post-transfection with siRNA p53, p53 protein was successfully depleted (Fig. 5A and B). AGR2 protein expression was also analyzed using Western blot (Fig 5A and C). We found that AGR2 expression, in the presence or absence of siRNA p53, was not modified (Fig 5C). Concomitantly, a sharper decrease of $p21^{CIP1}$ expression in HBEC overexpressing AGR2 (HBEC-AGR2) cells was observed upon treatment of those cells with the p53 siRNA compared to the ctl siRNA and to HBEC cells transfected with the p53 siRNA (Fig 5D). Our results demonstrate that AGR2 gain and p53 lost inhibit $p21^{CIP1}$ expression and that both together further decrease $p21^{CIP1}$ expression, suggesting the hypothesis of a p53-independent $p21^{CIP1}$ inhibition by AGR2.

To confirm our hypothesis that $p21^{CIP1}$ inhibition could be triggered by AGR2 through p53-independent mechanisms, we investigated the expression of AGR2, p53 and $p21^{CIP1}$ in clinical samples of lung cancer patients using immunohistochemistry (Table 2). We evaluated the expression of AGR2, p53 and $p21^{CIP1}$ protein in adjacent non-tumour (ANT) and tumour tissue (T) samples at different stages (Fig. 5E). Immunohistochemistry revealed that AGR2, p53 and $p21^{CIP1}$ were significantly overexpressed in tumour tissue (T) as compared to adjacent non-tumour tissue (ANT) (Fig. 5F). Pearson correlation analysis showed that there was no significant correlation between AGR2 and p53 expression levels in tumour tissue (T) (Fig. 5G). In contrast, there was a significant negative correlation between AGR2 and $p21^{CIP1}$ expression levels ($r = -0.2838$, $p=0.0394$) in tumour tissue (T) (Fig. 5H). Together, these results confirm our initial hypothesis that $p21^{CIP1}$ inhibition could be mediated by AGR2 through p53-independent mechanisms.

To further investigate the AGR2 cell signalling pathway which mediates the p53-independent inhibition of $p21^{CIP1}$ expression, we monitored the phosphorylation of AKT that

has been consistently reported to regulate negatively $p21^{CIP1}$ expression [24]. Moreover, it was suggested that AGR2 overexpression may result in AKT phosphorylation [25]. As such, AKT expression and phosphorylation levels were determined in HBEC and HBEC-AGR2-WT cells using Western blotting (Fig. 5I). Results indicated that AGR2 expression did not modify AKT phosphorylation and thus support that the $p21^{CIP1}$ inhibition by AGR2 is Akt independent. It has been also demonstrated that overexpression of c-Myc negatively regulates $p21^{CIP1}$ expression [24], and that AGR2 may stimulate c-Myc expression [26]. Thus, c-Myc expression levels were determined in HBEC as compared to HBEC-AGR2-WT cells using Western blotting (Fig. 5I). Results indicated that AGR2 expression did not impact c-Myc levels supporting that the $p21^{CIP1}$ inhibition by AGR2 is c-Myc independent. We next addressed whether the reduction of $p21^{CIP1}$ expression was also observed at the transcriptional level. We compared the $p21^{CIP1}$ mRNA expression levels in HBEC and HBEC overexpressing AGR2 (HBEC-AGR2) using RT-PCR (Fig. 5J). We found that $p21^{CIP1}$ mRNA expression was not affected by the overexpression of AGR2. Since it was reported that the degradation of $p21^{CIP1}$ is regulated by the ubiquitin/proteasome pathway [27], we hypothesized that the reduction of $p21^{CIP1}$ induced by AGR2 might be proteasome-mediated. We demonstrated that MG132 enhanced the expression level of $p21^{CIP1}$ in HBEC and HBEC-AGR2-WT cells (Fig. 5K), which suggests that the reduction of $p21^{CIP1}$ expression is most likely due to protein degradation. Collectively, our results demonstrate that AGR2 regulates the expression of $p21^{CIP1}$ mostly at the post-translational level.

3.8. Extracellular AGR2 (eAGR2) promotes tumour cell growth through $p21^{CIP1}$ *inhibition.*

We recently showed that the ER-resident chaperone AGR2, involved in ER protein folding and quality control, is secreted by lung tumour cells in the tumour microenvironment (extracellular AGR2 (eAGR2)), and exerts signalling tumour-associated properties [1, 2]. Immunostaining of three non-permeabilized lung cancer cell lines (A549, H23 and H1838) (Fig. 6A), indicated that eAGR2, present in the tumour microenvironment, was also localized at the external surface of the plasma membrane of lung cancer cells (Fig. 6A). Recently, we have demonstrated that the addition of eAGR2 to the medium of AGR2-depleted lung cancer cell lines reversed the cell growth inhibition induced by AGR2 depletion [2]. Therefore, we sought to determine whether there was any relation between eAGR2 and $p21^{CIP1}$. As expected, the addition of eAGR2 to the microenvironment of A549-AGR2 depleted cells

(A549-ShAGR2) restored tumour cell proliferation (Fig. 6B and C). Interestingly, decreased $p21^{CIP1}$ protein expression was also observed in the presence of eAGR2 in the microenvironment (Fig. 6D), which correlated with the restoration of A549-AGR2 depleted cell proliferation (Fig. 6B and C). Collectively, these data demonstrate that i) the AGR2 binds to the plasma membrane, and ii) eAGR2 signals to yield $p21^{CIP1}$ expression attenuation and to enhance cell proliferation.

4. Discussion

Anterior GRadient (AGR) protein family members are involved in several tumour-associated processes such as differentiation, proliferation, migration, invasion and metastasis [1, 3, 28, 29]. Several reports demonstrated that altered AGR protein expression plays a crucial role in the progression of multiple human cancers [1, 3, 28, 30]. As a critical member of the AGR family, AGR2 has been reported to be highly expressed and to play a role in the progression of various adenocarcinomas [1-5]. However, the function of AGR2 in tumour development remains to be fully elucidated.

Herein, we observed that AGR2 localized to both the conducting airways and the acini of the lung tree and was highly expressed in lung tumour tissues when compared with paired non-tumour tissues, which agrees with previous studies in lung cancer and other epithelial cancers [1-4]. These data suggest that AGR2 might play a role in the progression of lung cancer and could function as a potential clinical prognostic predictor for lung cancer patients. The progression of lung cancer is accompanied or driven by unlimited proliferation and metastasis of cancer cells. We and others reported that AGR2 participates in those two above-mentioned processes [1-3]. Our present data show that tumour cell proliferation is reduced when AGR2 is depleted in lung cancer cells. As well, we have demonstrated that the depletion of AGR2 led to a reduction in lung cancer growth *in vivo* [2]. These findings indicate that AGR2 may contribute to the progression of lung cancer by promoting tumour cell proliferation. AGR2 has two major functional domains: a dimerization domain (amino acids 60-64) [8] and a thioredoxin domain [2] (amino acids 81-84). In our cell growth tests, we showed that AGR2 promotes cell growth, independently of these two major functional domains. Thus, future work will be necessary to determine the AGR2 specific domain(s) necessary for promoting tumour cell growth.

In the present work, we focused on the possible involvement of the tumour suppressor $p21^{CIP1}$ in AGR2-mediated cell proliferation. We demonstrated that, in addition to the inhibition of lung cancer cell growth, down-regulation of AGR2 can lead to the up-regulation of $p21^{CIP1}$. In the same context, AGR2 overexpression in non-tumorigenic HBEC increased their proliferation and correlated with decreased $p21^{CIP1}$ expression. Our data *in vitro* and *in vivo* demonstrated an inverse correlation between AGR2 and $p21^{CIP1}$ expression levels and cell proliferation effects, independently of the influence of specific oncogenic lesions. We observed that the reduction of $p21^{CIP1}$ is regulated by the ubiquitin/proteasome system,

suggesting that AGR2 might participate to the activation of this pathway to degrade the $p21^{CIP1}$ protein. However, the details of such mechanism remain to be elucidated. Our results support that $p21^{CIP1}$ is decreased by AGR2 protein and involved in AGR2-mediated tumour cell growth progression via the regulation of cell cycle regulators and that AGR2 regulates the expression of $p21^{CIP1}$ at the post-translational level, in a p53-independent manner. Moreover, it has been shown that Rb is responsible for the major G1 checkpoint (restriction point) blocking S-phase entry and cell growth [31], which could explain the AGR2 effect on cell cycle following a scheme in which AGR2 increases the percentage of cells in G2-M and decreases those in G1.

Emerging data showed that AGR2 exists not only as a monomer but also can form an homodimeric structure [5-8, 32, 33]. We recently demonstrated that AGR2 homodimers act as sensors of ER homeostasis which are disrupted upon ER stress and promote the secretion of AGR2 monomers [8]. Based on the general theory that homeostasis of the secretory pathway represents a key factor in secretome control, it is likely that AGR2 may play a dual role in cancer development, first by exerting its expected protein folding functions in the ER (intracellular AGR2 (iAGR2)) and second through pro-oncogenic extracellular gain-of-functions (extracellular AGR2(eAGR2)) [1-5]. Thus, control of AGR2 dimerization could represent a relevant factor in cancer development. Furthermore, we provide the first evidence that AGR2 also localizes to the cell surface of lung cancer cell lines as previously demonstrated in some other cancer cells [1, 3]. Thus, eAGR2 could be a functional ligand for a receptor present at the surface of tumour lung epithelial cells, receptor which remains to be identified. Hence, as a secreted protein, eAGR2 could act through autocrine and/or paracrine mechanisms as a tumour growth factor (Fig. 7). However, the growth factor signalling transduction by which eAGR2 may exert its cell tumour growth progression effect remains to be characterized (Fig. 7).

It remains to determine whether eAGR2 acts in increasing cell tumour growth through direct or indirect activation of a plasma membrane receptor(s) and whether the eAGR2 receptor-signalling cascade represents a new tumour growth pathway (Fig. 7). Regardless of the upstream signalling components, it is clear that eAGR2 appears to increase tumour growth by promoting a decrease of $p21^{CIP1}$ protein expression, a hallmark of cancer [34]. This is further supported by our findings that the addition of eAGR2 in the medium of AGR2-depleted cells reverses cell growth inhibition and the increase of $p21^{CIP1}$ expression, both induced by AGR2 depletion.

In conclusion, our results shed light on a novel mechanism through which eAGR2 could be considered as a new type of tumour growth factor released in the tumour niche. AGR2 promotes tumour growth through the negative regulation of $p21^{CIP1}$ expression, independently of its ER function and through gain-of-extracellular functions (Fig. 7). Our results also suggest that targeting the eAGR2/p21-based signalling pathway should be further explored for its potential to decrease sustained proliferation in cancer and for identifying molecular targets that may provide early diagnostic markers and/or critical targets for the development of new anticancer drugs.

Conflict of interest statement

None declared

Acknowledgements

We gratefully acknowledge the members from ARTiSt group for their critical remarks. TG was supported by the Site de recherche intégrée sur le cancer de Bordeaux (SIRIC Brio). FD was supported by a grant from “Ligue contre le Cancer” (Comité Charente). This work has been supported by the Fondation ARC pour la recherche sur le cancer (FD). This work has been supported by the Agence Nationale de la Recherche (ANR) (DF). This work was also funded by grants from the Institut National du Cancer (INCa), Fondation pour la Recherche Médicale (FRM, équipe labellisée) and Agence Nationale de la Recherche (ANR) to EC.

References

[1] F. Delom, A. Nazaraliyev, D. Fessart, The role of protein disulphide isomerase AGR2 in the tumour niche, Biology of the cell, 110 (2018) 271-282.
[2] D. Fessart, C. Domblides, T. Avril, L.A. Eriksson, H. Begueret, R. Pineau, C. Malrieux, N. Dugot-Senant, C. Lucchesi, E. Chevet, F. Delom, Secretion of protein disulphide isomerase AGR2 confers tumorigenic properties, eLife, 5 (2016).
[3] E. Chevet, D. Fessart, F. Delom, A. Mulot, B. Vojtesek, R. Hrstka, E. Murray, T. Gray, T. Hupp, Emerging roles for the pro-oncogenic anterior gradient-2 in cancer development, Oncogene, 32 (2013) 2499-2509.
[4] A. Higa, A. Mulot, F. Delom, M. Bouchecareilh, D.T. Nguyen, D. Boismenu, M.J. Wise, E. Chevet, Role of pro-oncogenic protein disulfide isomerase (PDI) family member anterior gradient 2 (AGR2) in the control of endoplasmic reticulum homeostasis, The Journal of biological chemistry, 286 (2011) 44855-44868.
[5] F. Delom, M.A. Mohtar, T. Hupp, D. Fessart, The AGR2 interactome, American journal of physiology. Cell physiology, (2019).
[6] P. Patel, C. Clarke, D.L. Barraclough, T.A. Jowitt, P.S. Rudland, R. Barraclough, L.Y. Lian, Metastasis-promoting anterior gradient 2 protein has a dimeric thioredoxin fold structure and a role in cell adhesion, Journal of molecular biology, 425 (2013) 929-943.
[7] D.J. Clarke, E. Murray, J. Faktor, A. Mohtar, B. Vojtesek, C.L. MacKay, P.L. Smith, T.R. Hupp, Mass spectrometry analysis of the oxidation states of the pro-oncogenic protein anterior gradient-2 reveals covalent dimerization via an intermolecular disulphide bond, Biochimica et biophysica acta, 1864 (2016) 551-561.
[8] M. Maurel, J. Obacz, T. Avril, Y.P. Ding, O. Papadodima, X. Treton, F. Daniel, E. Pilalis, J. Horberg, W. Hou, M.C. Beauchamp, J. Tourneur-Marsille, D. Cazals-Hatem, L. Sommerova, A. Samali, J. Tavernier, R. Hrstka, A. Dupont, D. Fessart, F. Delom, M.E. Fernandez-Zapico, G. Jansen, L.A. Eriksson, D.Y. Thomas, L. Jerome-Majewska, T. Hupp, A. Chatziioannou, E. Chevet, E. Ogier-Denis, Control of anterior GRadient 2 (AGR2) dimerization links endoplasmic reticulum proteostasis to inflammation, EMBO molecular medicine, 11 (2019).
[9] F. Delom, A. Nazaraliyev, D. Fessart, The role of protein disulphide isomerase AGR2 in the tumour niche, Biology of the cell, (2018).
[10] D. Fessart, H. Begueret, F. Delom, Three-dimensional culture model to distinguiSh normal from malignant human bronchial epithelial cells, The European respiratory journal, 42 (2013) 1345-1356.
[11] F. Delom, I. Begiristain, T. Grenier, H. Begueret, F. Soulet, G. Siegfried, A.M. Khatib, J. Robert, D. Fessart, Patients Lung Derived Tumoroids (PLDTs) to model therapeutic response, Biochimica et biophysica acta. Molecular cell research, 1867 (2020) 118808.
[12] F. Delom, P.J. Lejeune, L. Vinet, P. Carayon, B. Mallet, Involvement of oxidative reactions and extracellular protein chaperones in the rescue of misassembled thyroglobulin in the follicular lumen, Biochemical and biophysical research communications, 255 (1999) 438-443.
[13] F. Delom, B. Mallet, P. Carayon, P.J. Lejeune, Role of extracellular molecular chaperones in the folding of oxidized proteins. Refolding of colloidal thyroglobulin by protein disulfide isomerase and immunoglobulin heavy chain-binding protein, The Journal of biological chemistry, 276 (2001) 21337-21342.
[14] H. Dihazi, G.H. Dihazi, A. Bibi, M. Eltoweissy, C.A. Mueller, A.R. Asif, D. Rubel, R. Vasko, G.A. Mueller, Secretion of ERP57 is important for extracellular matrix accumulation and progression of renal fibrosis, and is an early sign of disease onset, Journal of cell science, 126 (2013) 3649-3663.
[15] T. Ilani, A. Alon, I. Grossman, B. Horowitz, E. KartveliShvily, S.R. Cohen, D. Fass, A secreted disulfide catalyst controls extracellular matrix composition and function, Science, 341 (2013) 74-76.
[16] V. Borgdorff, M.E. Lleonart, C.L. BiShop, D. Fessart, A.H. Bergin, M.G. Overhoff, D.H. Beach, Multiple microRNAs rescue from Ras-induced senescence by inhibiting p21(Waf1/Cip1), Oncogene, 29 (2010) 2262-2271.
[17] D. Fessart, M.L. Martin-Negrier, S. Claverol, M.L. Thiolat, H. Crevel, C. Toussaint, M. Bonneu, B. Muller, J.P. Savineau, F. Delom, Proteomic remodeling of proteasome in right heart failure, Journal of molecular and cellular cardiology, 66 (2014) 41-52.
[18] D. Fessart, M. Simaan, S.A. Laporte, c-Src regulates clathrin adapter protein 2 interaction with

beta-arrestin and the angiotensin II type 1 receptor during clathrin- mediated internalization, Molecular endocrinology, 19 (2005) 491-503.
[19] F. Delom, D. Fessart, E. Chevet, Regulation of calnexin sub-cellular localization modulates endoplasmic reticulum stress-induced apoptosis in MCF-7 cells, Apoptosis : an international journal on programmed cell death, 12 (2007) 293-305.
[20] M. Maurel, J. Obacz, T. Avril, Y.P. Ding, O. Papadodima, X. Treton, F. Daniel, E. Pilalis, J. Horberg, W. Hou, M.C. Beauchamp, J. Tourneur-Marsille, D. Cazals-Hatem, L. Sommerova, A. Samali, J. Tavernier, R. Hrstka, A. Dupont, D. Fessart, F. Delom, M.E. Fernandez-Zapico, G. Jansen, L.A. Eriksson, D.Y. Thomas, L. Jerome-Majewska, T. Hupp, A. Chatziioannou, E. Chevet, E. Ogier-Denis, Control of anterior GRadient 2 (AGR2) dimerization links endoplasmic reticulum proteostasis to inflammation, EMBO molecular medicine, (2019).
[21] A. Karimian, Y. Ahmadi, B. Yousefi, Multiple functions of p21 in cell cycle, apoptosis and transcriptional regulation after DNA damage, DNA repair, 42 (2016) 63-71.
[22] E. Pohler, A.L. Craig, J. Cotton, L. Lawrie, J.F. Dillon, P. Ross, N. Kernohan, T.R. Hupp, The Barrett's antigen anterior gradient-2 silences the p53 transcriptional response to DNA damage, Molecular & cellular proteomics : MCP, 3 (2004) 534-547.
[23] S. Courtois-Cox, S.L. Jones, K. Cichowski, Many roads lead to oncogene-induced senescence, Oncogene, 27 (2008) 2801-2809.
[24] B. Shamloo, S. Usluer, p21 in Cancer Research, Cancers, 11 (2019).
[25] A. Dong, A. Gupta, R.K. Pai, M. Tun, A.W. Lowe, The human adenocarcinoma-associated gene, AGR2, induces expression of amphiregulin through Hippo pathway co-activator YAP1 activation, The Journal of biological chemistry, 286 (2011) 18301-18310.
[26] K.E. Vanderlaag, S. Hudak, L. Bald, L. Fayadat-Dilman, M. Sathe, J. Grein, M.J. Janatpour, Anterior gradient-2 plays a critical role in breast cancer cell growth and survival by modulating cyclin D1, estrogen receptor-alpha and survivin, Breast cancer research : BCR, 12 (2010) R32.
[27] J. Bloom, V. Amador, F. Bartolini, G. DeMartino, M. Pagano, Proteasome-mediated degradation of p21 via N-terminal ubiquitinylation, Cell, 115 (2003) 71-82.
[28] J. Obacz, M. Takacova, V. Brychtova, P. Dobes, S. Pastorekova, B. Vojtesek, R. Hrstka, The role of AGR2 and AGR3 in cancer: similar but not identical, European journal of cell biology, 94 (2015) 139-147.
[29] V. Brychtova, A. Mohtar, B. Vojtesek, T.R. Hupp, Mechanisms of anterior gradient-2 regulation and function in cancer, Seminars in cancer biology, 33 (2015) 16-24.
[30] J. Obacz, L. Sommerova, D. Sicari, M. Durech, T. Avril, F. Iuliano, S. Pastorekova, R. Hrstka, E. Chevet, F. Delom, D. Fessart, Extracellular AGR3 regulates breast cancer cells migration via Src signaling, Oncology letters, 18 (2019) 4449-4456.
[31] M. Hatakeyama, R.A. Weinberg, The role of RB in cell cycle control, Progress in cell cycle research, 1 (1995) 9-19.
[32] J. Ryu, S.G. Park, P.Y. Lee, S. Cho, D.H. Lee, G.H. Kim, J.H. Kim, B.C. Park, Dimerization of pro-oncogenic protein Anterior Gradient 2 is required for the interaction with BiP/GRP78, Biochemical and biophysical research communications, 430 (2013) 610-615.
[33] T.A. Gray, E. Murray, M.W. Nowicki, L. Remnant, A. Scherl, P. Muller, B. Vojtesek, T.R. Hupp, Development of a fluorescent monoclonal antibody-based assay to measure the allosteric effects of synthetic peptides on self-oligomerization of AGR2 protein, Protein science : a publication of the Protein Society, 22 (2013) 1266-1278.
[34] D. Hanahan, R.A. Weinberg, Hallmarks of cancer: the next generation, Cell, 144 (2011) 646-674.

Table 1: Overview of the Investigated Lung Cancer Cohort for AGR2 expression

Characteristics	N° of Patients (n=90)	Percentage	Age		Sex	
			<60.12	>60.12	Male	Female
Age			53	37	58	32
Mean (SD), y	61.38 (9.68)				62.2	59.8
Median, y	62				62	61
Range, y	38-82				38-80	39-82
Gender						
Male	58	64.4%	25 (27.7%)	33 (36.6)		
Female	32	35.5%	14 (15.5%)	18 (20%)		
Histologic Type						
Adenocarcinoma	73	81.1%	29 (32.2%)	44 (48.8%)	44 (48.8%)	29 (32.8%)
Squamous cell lung carcinoma	14	15.5%	7 (7.7%)	7 (7.7%)	13 (14.4%)	1 (1.1%)
Other	3	3.3%	3 (3.3%)	0	1 (1.1%)	2 (2.2%)
Stage						
I-II	34	37.6%	12 (13.2%)	22 (24.2%)	21 (23.3%)	13 (14.3%)
III-IV	52	57.7%	23 (25.5%)	28 (31.1%)	36 (39.9%)	16 (17.7%)

Table 2: Patients Characteristics for AGR2, p53 and p21 ^{CIP1} Pearson's correlation

Characteristics	N° of Patients (n=56)	Percentage	Age		Sex	
			<63.16	>63.16	Male	Female
Age			27	29	32	24
Mean (SD), y	63.16 (9.92)				61.1 (11)	61.8 (8.1)
Median, y	62.5				65	62

Range, y	39-82				39-82	48-80
Gender						
Male	32	57.14%	15 (55.5%)	10 (34.4)		
Female	24	42.85%	12 (44.4%)	19 (65.5%)		
Histologic Type						
Adenocarcinoma	56	100%	27 (100%)	29 (100%)	32 (100%)	24 (100%)
Stage						
I-II	25	44.63%	10(37%)	15 (52.9%)	14 (43.6%)	11 (45.8%)
III-IV	28	59.9%	16 (59.2%)	12 (43.1%)	18 (56.2%)	13(54.1%)

Figure 1

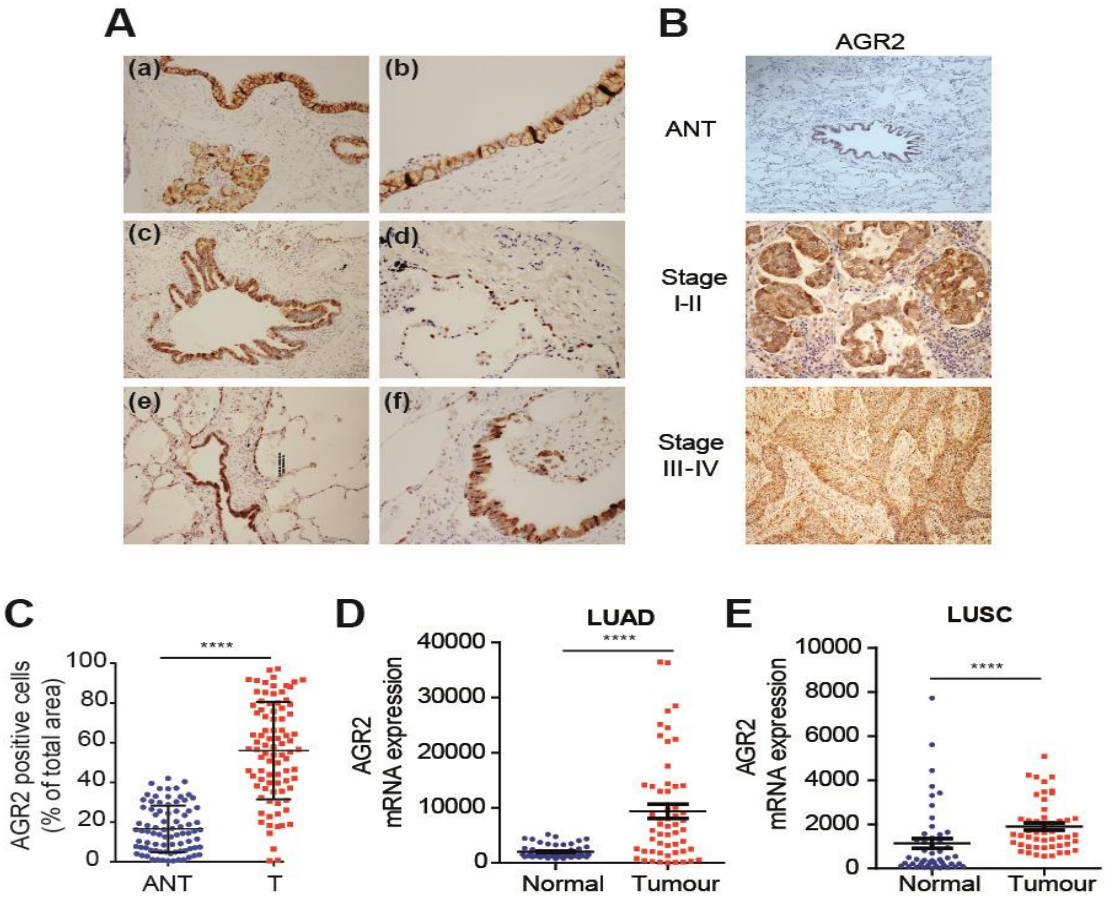

Fig. 1. AGR2 expression in human bronchial tree and lung cancer.

(**A**) Human bronchial tree showing in (a), proximal bronchia with a strong AGR2 staining localized to mucinous and ciliated cells of the respiratory epithelium (×100). Representative pictures: in (b) of proximal bronchia (×200), in (c) terminal bronchiola, in (e) respiratory bronchiola and in (f) respiratory bronchiola (×100). AGR2 staining is similar to respiratory epithelium from proximal bronchia to a distal terminal and respiratory bronchiolar structures. In (d) representative pictures of sub-pleural alveolar parenchyma with a strong AGR2 expression by type 2 pneumocytes (×100).

(**B**) AGR2 expression determined by immunohistochemistry in sections of formalin-fixed paraffin-embedded lung cancer tissues from patients at different stages as compared to adjacent non-tumour tissues (ANT) (×100).

(**C**) Box plot of the statistical analysis of the percentage of AGR2 positive cells between

tumour (T) and corresponding non-tumour (ANT) tissues. **** indicates p<0.0001 (Student's t-test).

(**D**) AGR2 expression in 56 tumour samples from TCGA database compared with paired adjacent normal tissue in lung adenocarcinoma (LUAD)($p = 2x10^{-4}$). An outlier value has been withdrawn from the tumour samples data.

(**E**) AGR2 expression in 50 tumour samples from TCGA database compared with paired adjacent normal tissue in lung squamous cell carcinomas (LUSC) ($p = 8.4x10^{-7}$). An outlier value has been withdrawn from the normal samples data.

Figure 2

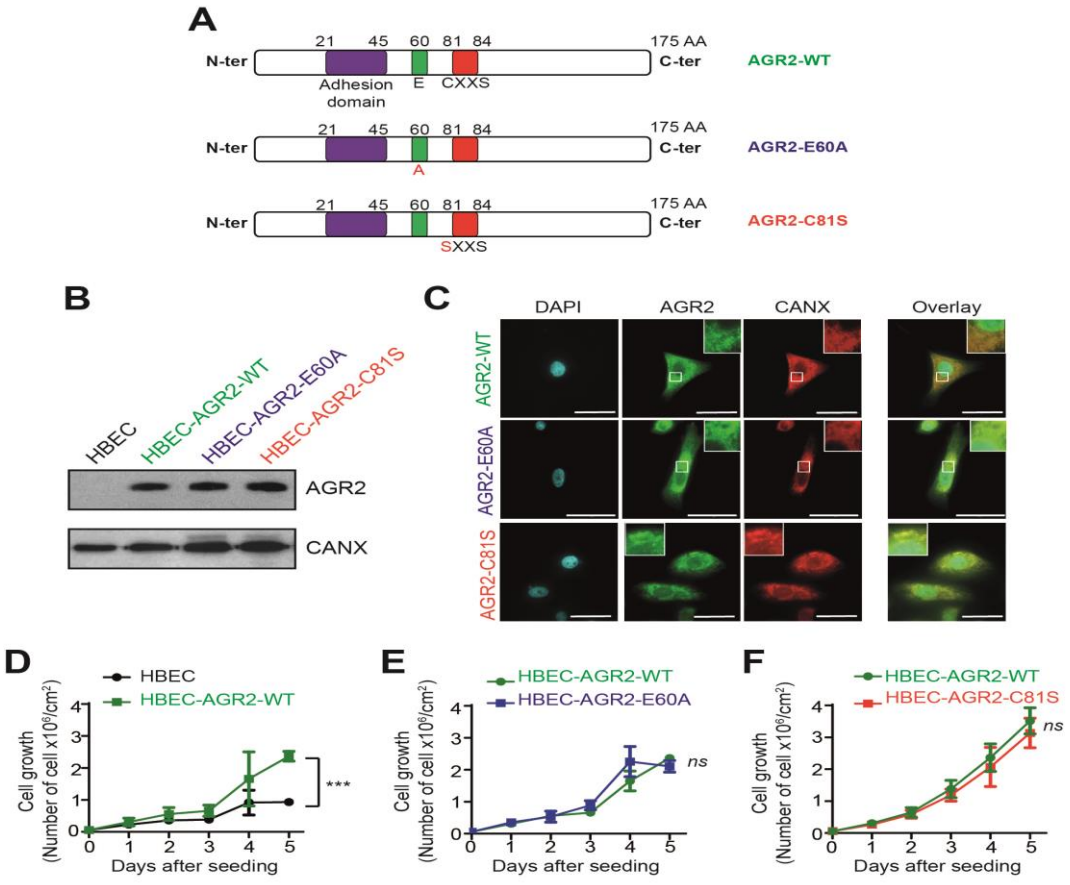

Fig.2. Effects of AGR2 and its different constructs on cell growth.

(**A**) Schematic representation of AGR2 point mutants (blue: adhesion domain, red: thioredoxin-like domain).

(**B**) Western blot analysis showing the overexpression of AGR2 wild-type and constructs in HBEC: AGR2-WT wild type (green), AGR2-E60A (blue) or AGR2-C81S (red). One representative experiment (n = 3) is shown.

(**C**) Analysis of AGR2 subcellular localization in infected HBECs by immunofluorescence. In the top corner, an enlarged area of the staining is shown. Calnexin (CANX) is used as an ER localisation control. Scale bars: 50 μm.

(**D**) Growth curves monitored in 96-well plates of HBEC cells stably expressing AGR2 wild-type (HBEC-AGR2) as compared to empty vector (HBEC). Cell growth was evaluated by measuring the cell number per field with a multi-mode microplate reader Cytation 3. Data are mean ± SEM of at least three independent experiments. *** indicates $p<0.001$ (two-way ANOVA).

(**E and F**) Growth curves monitored in 96-well plates of HBEC cells stably expressing AGR2 constructs (AGR2-E60A (E) and AGR2- C81S (F)) as compared to HBEC-AGR2. Cell growth was evaluated by measuring the cell number per field with a multi-mode microplate reader Cytation 3. Data are mean ± SEM of at least three independent experiments. Non-significant: *ns*.

Figure 3

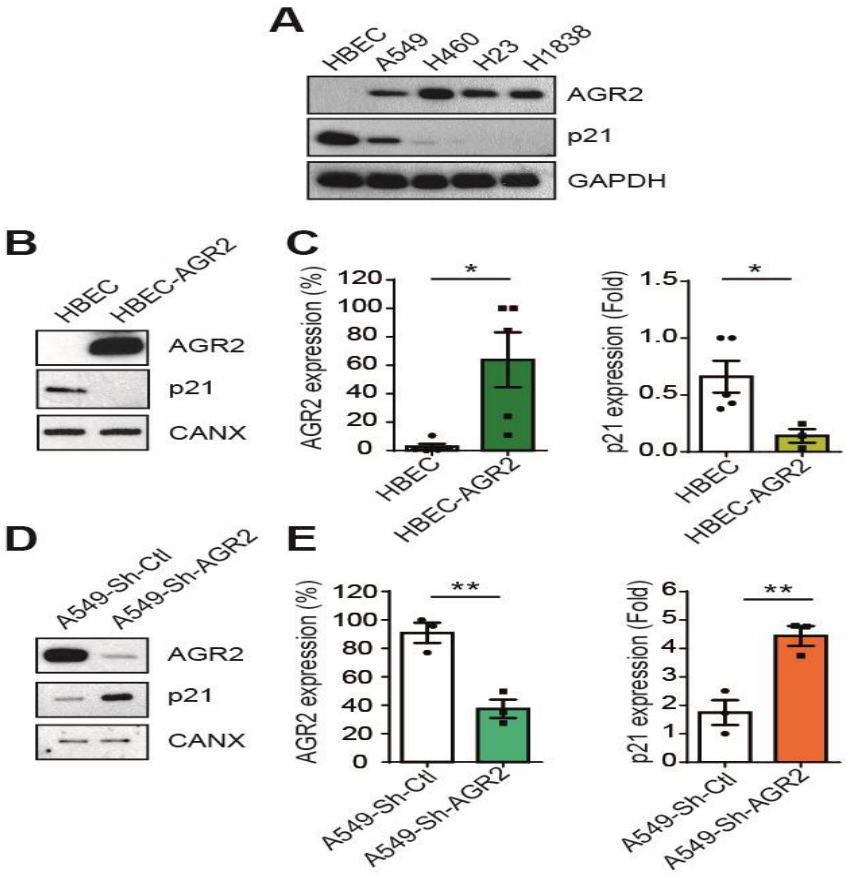

Figure 3: AGR2 affects p21 expression levels.

(A) Expression of AGR2 and $p21^{CIP1}$ protein levels by Western blot in normal HBEC and a panel of human lung cancer cell lines (A549, H460, H23 and H1838).

(**B**) Western blot analysis of $p21^{CIP1}$ protein levels in HBEC as compared to HBEC infected with AGR2 (HBEC-AGR2). Calnexin (CANX) concentrations are shown as a loading control. One representative experiment (n = 3) is shown.

(**C**) Quantification of the relative signal intensity of AGR2 and $p21^{CIP1}$ normalized to calnexin levels (CANX) from AGR2 overexpressing and control HBEC lysates. Data are mean ± SEM. * indicates $p<0.05$ (Student's t-test).

(**D**) Western blot analysis of $p21^{CIP1}$ protein levels in A549 lung cancer cells (A549-Sh-Ctl) and AGR2-depleted A549 cells (A549-Sh-AGR2). Calnexin (CANX) concentrations are

shown as a loading control. One representative experiment (n = 3) is shown.

(**E**) Quantification of the relative signal intensity of AGR2 and p21^{CIP1} normalised to calnexin levels (CANX) from AGR2-depleted and control A549 lysates. Data are mean ± SEM. ** indicates p<0.01 (Student's t-test).

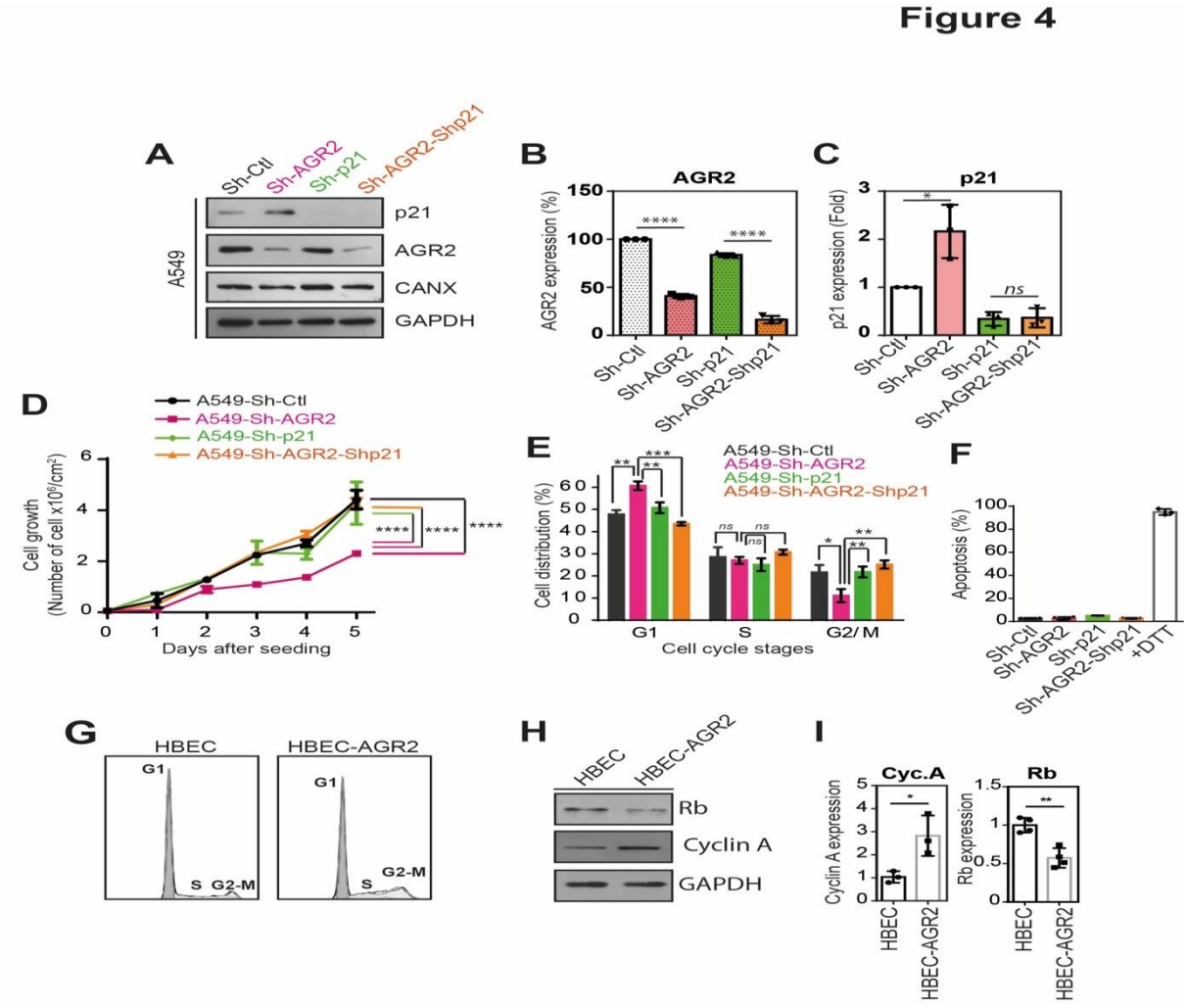

Figure 4: Downregulation of p21 reverses the cell growth inhibition induced by AGR2 knockdown.

(A) Western blot analysis showing the p21^{CIP1} protein levels in A549 control cells (A549-Sh-Ctl), in AGR2-depleted A549 cells (A549-Sh-AGR2) as compared to p21-depleted A549 cells (A549-Sh-p21) and AGR2/p21-depleted A549 cells (A549-Sh-AGR2-Sh-p21). Calnexin (CANX) and GAPDH concentrations are shown as a loading control. One representative experiment (n = 3) is shown.

(**B and C**) Histograms showing the quantification of the relative signal intensity of AGR2 (B)

or p21 (C) in the different cell lines (A549-Sh-Ctl, A549-Sh-AGR2, A549-Sh-p21, A549-Sh-AGR2-Sh-p21) from at least three independent biological replicates. The statistical analysis was performed between Sh-Ctl and Sh-AGR2; and between Sh-p21 and Sh-AGR2-Shp21. * indicates $p<0.05$, and ****indicates $p<0.0001$, *ns* not significant (Student's t-test).

(**D**) Growth curves monitored in 96-well plates of A549 cells depleted with Sh-control (A549-Sh-Ctl, black), with Sh-AGR2 (A549-Sh-AGR2, pink), with Sh-p21 (A549-Sh-p21, green) and with Sh-AGR2 and Sh-p21 (A549-Sh-AGR2-Shp21, orange). Cell growth was evaluated by measuring the cell number per field with a multi-mode microplate reader Cytation 3. Data are mean ± SEM of at least three independent experiments. **** indicates $p<0.0001$ (two-way ANOVA).

(E) Cell cycle analysis was performed in A549 cells depleted with Sh-control (A549-ShCtl), AGR2-depleted A549 cells (A549-Sh-AGR2) as compared to p21-depleted A549 cells (A549-Sh-p21) and AGR2/p21-depleted A549 cells (A549-Sh-AGR2-Sh-p21). Cells were stained with propidium iodide (PI). The DNA content was analyzed using flow cytometry with FlowJo software. The histogram shows the flow cytometry analysis. Results are representative of 3 independent experiments. *$p<0.05$, **$p<0.01$.Data are mean ± SEM of at least three independent experiments. * indicates $p<0.05$, ** indicates $p<0.01$ and ***indicates $p<0.001$, ns not significant (Student's t-test).

(**F**) Quantitation of cell death performed in A549 cells depleted with Sh-control (A549-Sh-Ctl), AGR2-depleted A549 cells (A549-Sh-AGR2) as compared to p21-depleted A549 cells (A549-Sh-p21) and AGR2/p21-depleted A549 cells (A549-Sh-AGR2-Sh-p21). Results are representative of three independent experiments. The cell death rate was determined with NucGreen (a marker of dead cells) and Nucblue (nuclei marker) as described in Materials and methods. DTT is used as a positive control for apoptosis.

(G) Cell cycle analysis was performed in HBEC as compared to HBEC overexpressing AGR2 (HBEC-AGR2). Cells were stained with propidium iodide (PI). The DNA content was analyzed using flow cytometry with FlowJo software. Results are representative of 3 independent experiments.

(H) Western blot analysis of Rb and cyclin A protein levels in HBEC as compared to HBEC overexpressing AGR2 (HBEC-AGR2). GAPDH is shown as a loading control. One representative experiment of 3 independent replicates (n = 3) is shown.

(I) Quantification of the relative signal intensity of Cyclin A and Rb normalized to GAPDH from AGR2 overexpressing and control HBEC lysates. Data are mean ± SEM of 3 independent replicates. Data are mean ± SEM of at least three independent experiments. * indicates $p<0.05$, ** indicates $p<0.01$ (Student's t-test).

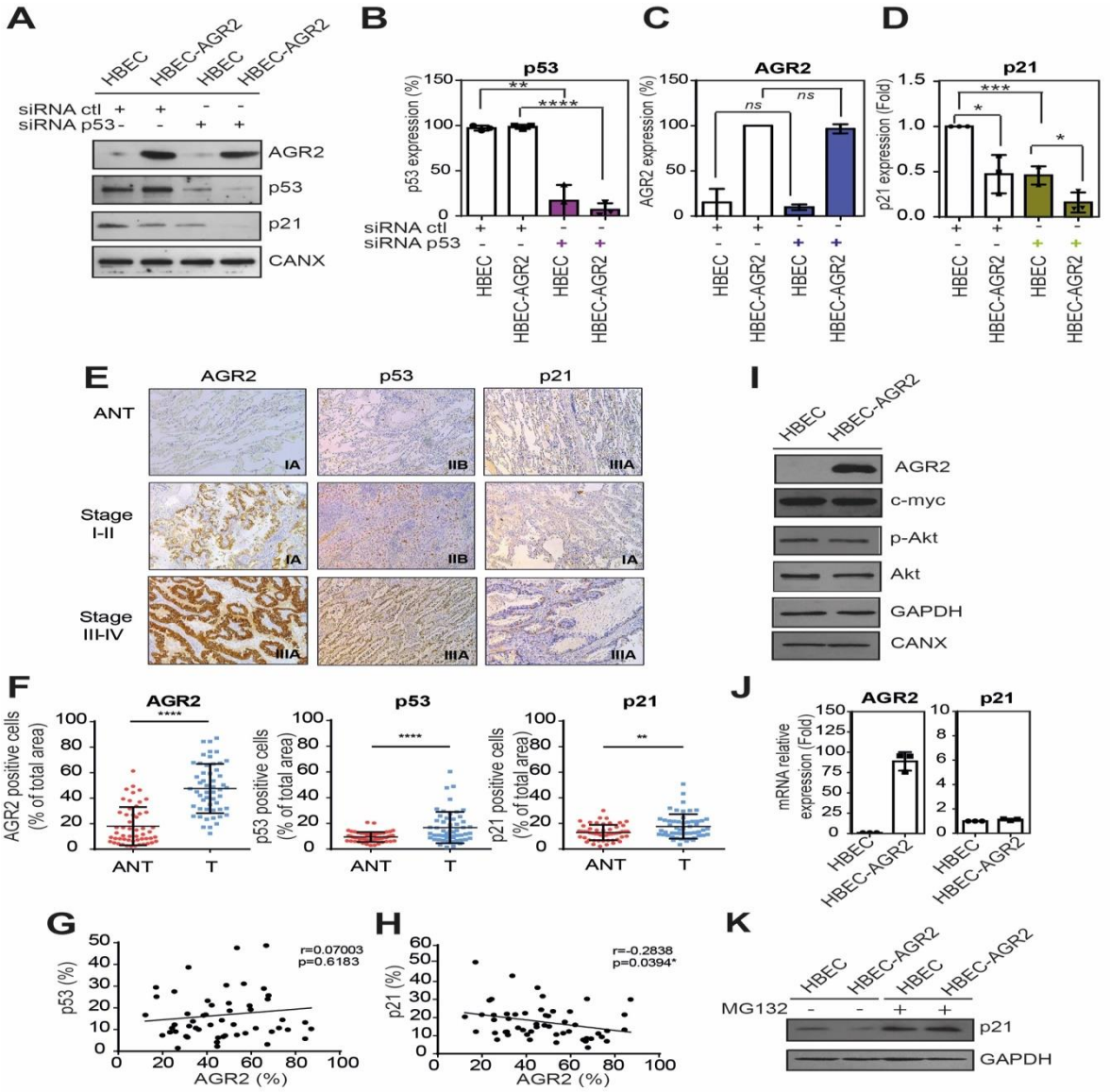

Figure 5: AGR2 induces a p53-independent p21^{CIP1} repression.

(A) Western blot analysis of p53 and p21^{CIP1} protein levels in HBEC as compared to HBEC infected with AGR2 (HBEC-AGR2) treated by siRNA with siControl (siRNA ctl) and sip53 (siRNA p53) for 72 hours. Calnexin (CANX) concentrations are shown as a loading control. One representative experiment (n = 3) is shown.

(**B**) Quantification of the relative signal intensity of p53 normalized to calnexin levels (CANX) from AGR2 overexpressing and control HBEC lysates treated by siRNA with

siControl (siRNA ctl) and sip53 (siRNA p53) for 72 hours. Data are mean ± SEM of 3 independent replicates. ** indicates p<0.01 and ***indicates p<0.001 (Student's t-test).

(**C**) Quantification of the relative signal intensity of AGR2 normalized to calnexin levels (CANX) from AGR2 overexpressing and control HBEC lysates treated by siRNA with siControl (siRNA ctl) and sip53 (siRNA p53) for 72 hours. Data are mean ± SEM of 3 independent replicates. *ns*: not significant (Student's t-test).

(**D**) Quantification of the relative signal intensity of $p21^{CIP1}$ normalized to calnexin levels (CANX) from AGR2 overexpressing and control HBEC lysates treated by siRNA with siControl (siRNA ctl) and sip53 (siRNA p53) for 72 hours. Data are mean ± SEM of 3 independent replicates. *indicates p<0.05 and ***p<0.001 (Student's t-test).

(**E**) AGR2, p53 and $p21^{CIP1}$ expression determined by immunohistochemistry in sections of formalin-fixed, paraffin-embedded lung cancer tissues from patients at different stages as compared to adjacent non-tumour tissues (ANT) (×100).

(**F**) AGR2, p53 and $p21^{CIP1}$ immunohistochemistry were scored in tumour tissues (T) from lung cancer patients and corresponding non-tumour tissues (ANT). Data are presented in a box plot of the statistical analysis of the percentage of positive cells for AGR2, p53 and $p21^{CIP1}$ respectively. **** indicates p<0.0001, ** indicates p<0.01 (Student's t-test).

(G, H) Analysis of the correlation between AGR2 expression and p53 protein levels (C) or $p21^{CIP1}$ protein levels (D) in lung cancer patient tissues (n = 52). Each data point represents the value of an individual patient. Correlation was measured by Pearson's correlation test. * indicates $p < 0.05$.

(I) Western blot analysis of AKT, pAKT and c-Myc protein levels in HBEC as compared to HBEC overexpressing AGR2 (HBEC-AGR2). GAPDH and Calnexin (CANX) concentrations are shown as a loading control. One representative experiment of 3 independent replicates (n = 3) is shown.

(J) Relative mRNA level of AGR2 and p21 expression in HEBC-ctl as compared to HBEC-AGR2 as determined by real-time PCR. GAPDH was used as a housekeeping gene.

(K) Western blot analysis of $p21^{CIP1}$ protein levels in HBEC as compared to HBEC infected with AGR2 (HBEC-AGR2) treated by 10 µM of MG132 for 4 hours. GAPDH concentrations are shown as a loading control. One representative experiment (n = 3) is shown.

Figure 6

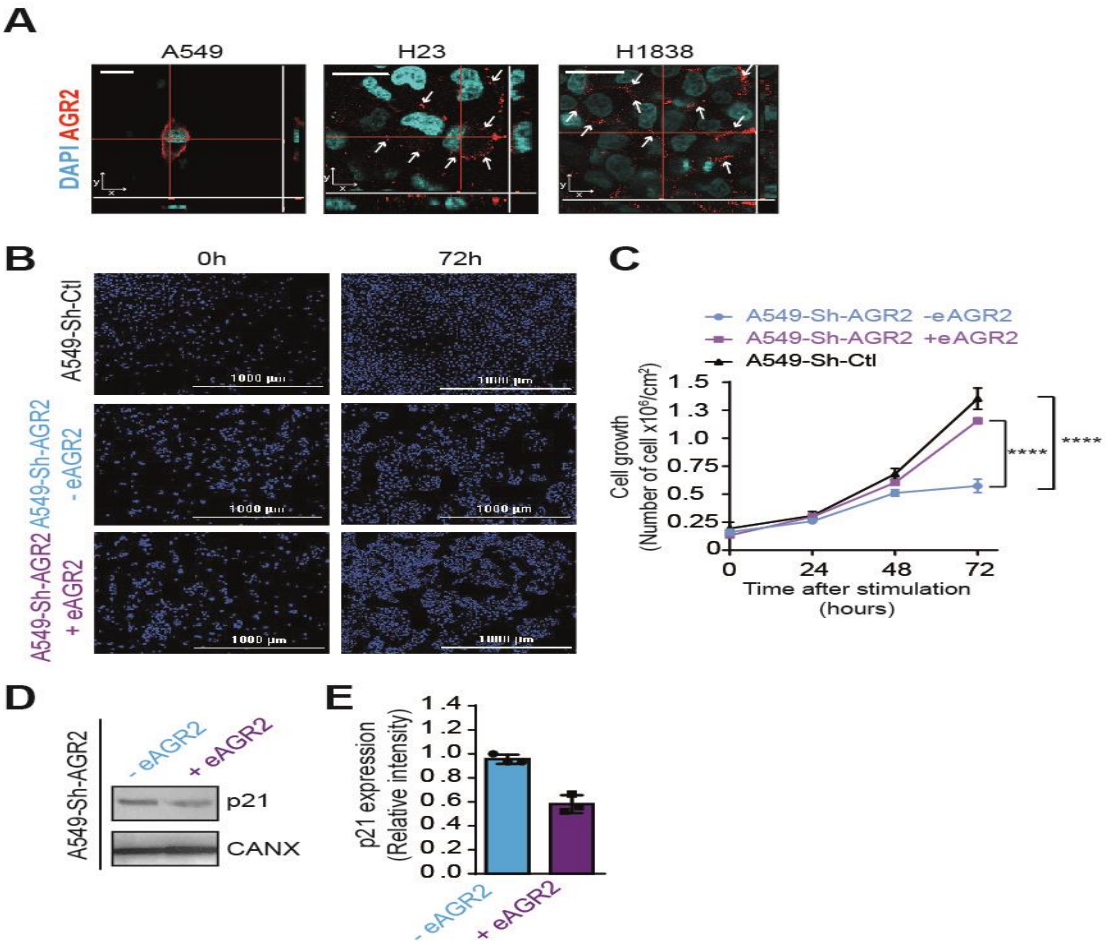

Figure 6: eAGR2 add-back rescues the cell growth inhibition induced by AGR2 knockdown via the regulation of p21^{CIP1}.

(A) Visualization by confocal microscopy of extracellular AGR2 (eAGR2) localization in lung cancer cells lines A549, H23 and H1838 respectively. Staining of AGR2 (red) and nuclei with DAPI (blue) were visualized. Z stacks along the x-and y-axes are presented at the bottom and on the right side of the images. AGR2 is localized to the cell surface membrane. White arrowheads indicate the AGR2 localized at the cell surface of the optical stack. Scale bar 50µm.

(**B**) Representative staining of nuclei with DAPI to measure the impact of eAGR2 on AGR2-depleted A549 cells growth following 72h of growth. Scale bar: 1000 µm.

(**C**) Growth curves monitored in 96 well plates of A549 cells depleted in Sh-control (Ctl) (A549-Sh-Ctl) as compared to A549 depleted in Sh-AGR2 (A549-Sh-AGR2) in the presence (+eAGR2) or not (-eAGR2) of eAGR2 in the cell medium. Cell growth was evaluated by measuring the cell number per field area with a multi-mode microplate reader Cytation 3. Data are mean ± SEM of at least three independent experiments. **** $p < 0.0001$ (two-way ANOVA).

(**D**) Western blot analysis Showing the $p21^{CIP1}$ protein levels in AGR2-depleted A549 (A549-Sh-AGR2) cells in the presence (+eAGR2) or absence (–eAGR2) of AGR2 in the extracellular medium. Calnexin (CANX) concentrations are shown as loading control. One representative experiment (n = 3) is shown.

(**E**) Quantification of the relative signal intensity of $p21^{CIP1}$ normalised to calnexin levels (CANX) from AGR2-depleted A549 cells (A549-Sh-AGR2) in the presence (+eAGR2) or absence (–eAGR2) of AGR2 in the extracellular medium. Data are mean ± SEM. ** indicates $p<0.01$ (Student's t-test).

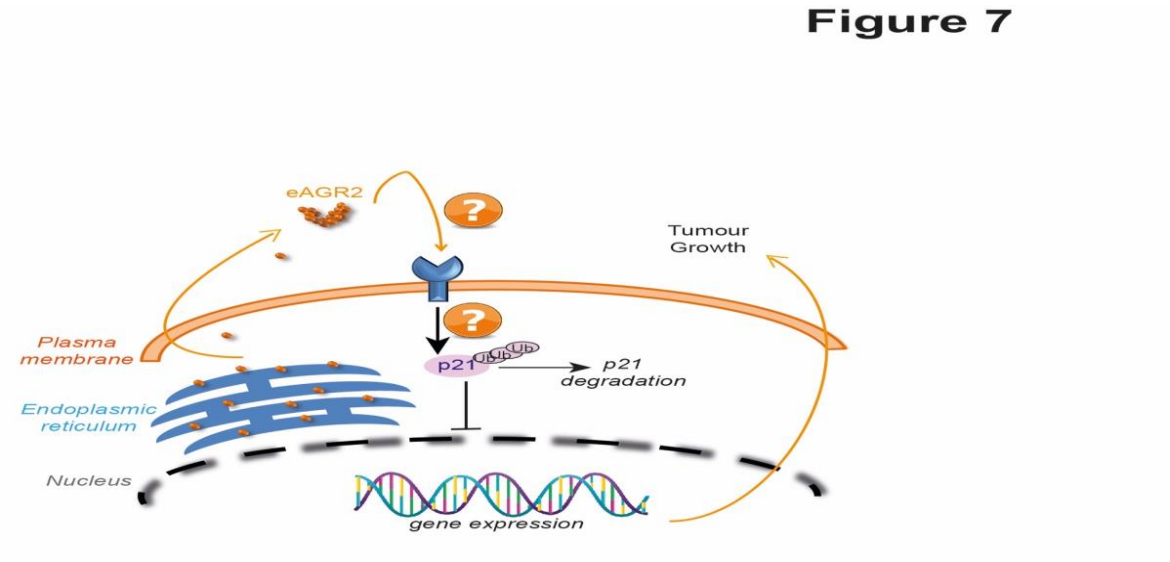

Figure 7: Proposed mechanism of action of eAGR2 in lung cancer cells to promote cell growth.

In lung cancer cells, the Endoplasmic Reticulum (ER)-resident protein anterior gradient-2 (AGR2), a soluble protein-disulfide isomerase which is involved in ER protein folding and quality control, is released through the secretome into the tumour niche. The extracellular AGR2 (eAGR2) binds the plasma membrane and presumably associates with a possible receptor. This binding should activate this cell surface receptor, followed by the initiation of an eAGR2 proteasome-dependent signalling cascade (still to be determined), and leading to $p21^{CIP1}$ degradation, thus promoting cancer cell proliferation and consequently tumour growth.

Declaration of competing interests

☐☐The authors declare that they have no known competing financial interests or personal relationships that could have appeared to influence the work reported in this paper.

☐The authors declare the following financial interests/personal relationships which may be considered as potential competing interests:

E.C. is a founding member of Cell Stress Discoveries Ltd. (https://cellstressdiscoveries.com/).

CRediT author statement

DF, CB, IB, TG, ER and **FD** carried out the experiments and related analyses. **DB** provided the reagents and critically revised the manuscript. **HB** provided and analyzed the biopsies. **EC** and **JR** critically revised the manuscript. **FD** and **DF** designed the study and wrote the manuscript. All authors read and approved the final manuscript.

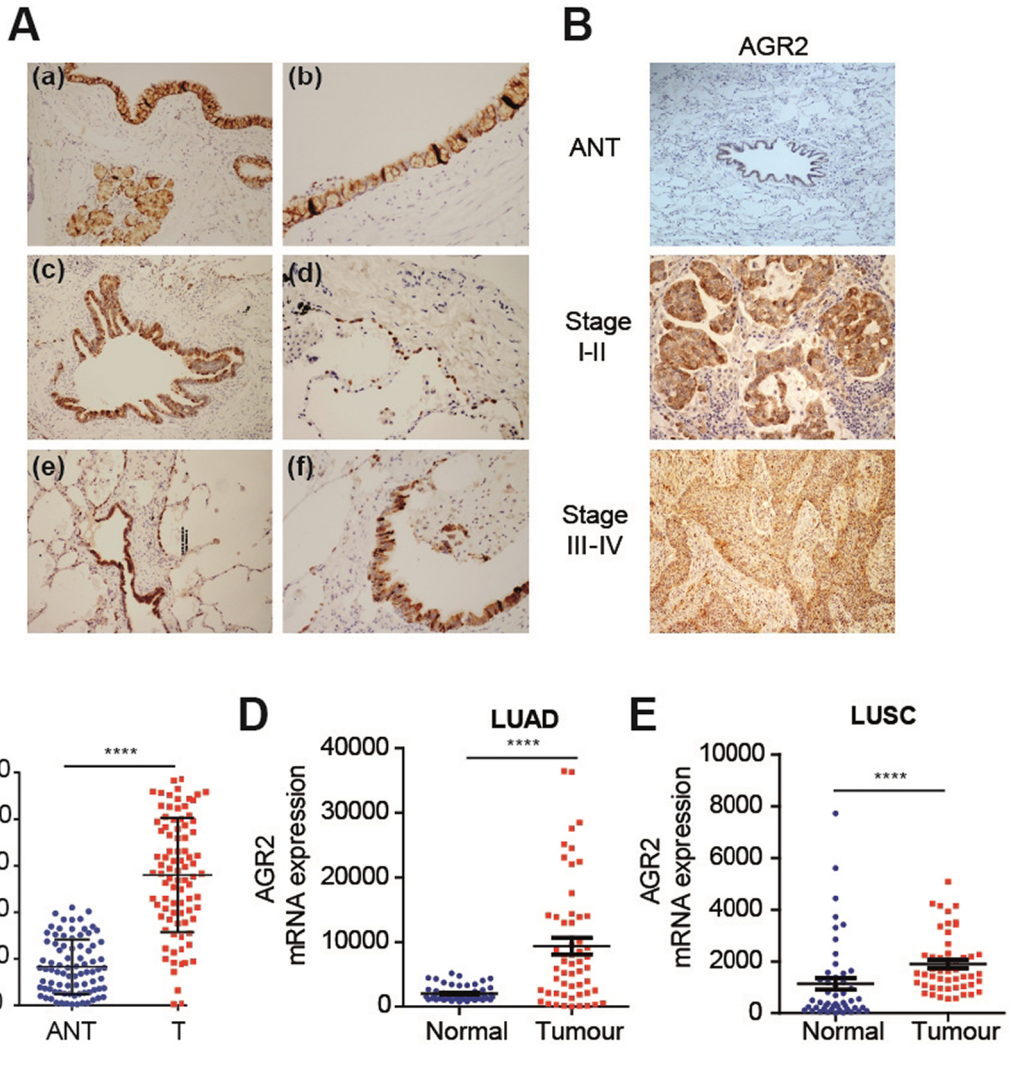
A
(a)
(b)
(c)
(d)
(e)
(f)
B
AGR2
ANT
Stage I-II
Stage III-IV
C
AGR2 positive cells (% of total area)
****
ANT
T
D
LUAD
AGR2 mRNA expression
****
Normal
Tumour
E
LUSC
AGR2 mRNA expression
****
Normal
Tumour

Figure 1

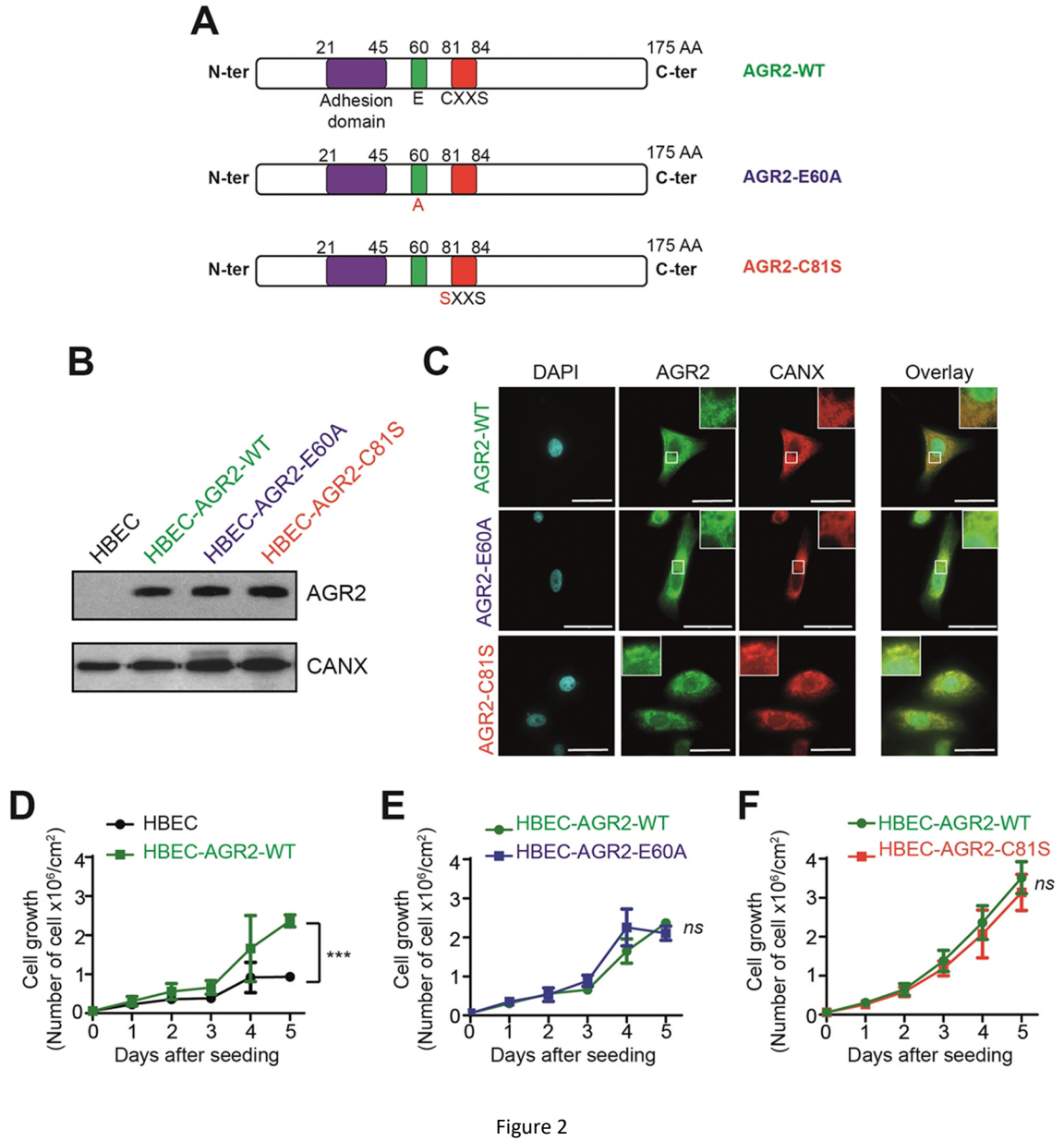
A
21 45 60 81 84
175 AA
N-ter
C-ter
Adhesion domain
E
CXXS
AGR2-WT
A
AGR2-E60A
SXXS
AGR2-C81S
B
HBEC
HBEC-AGR2-WT
HBEC-AGR2-E60A
HBEC-AGR2-C81S
AGR2
CANX
C
DAPI
AGR2
CANX
Overlay
AGR2-WT
AGR2-E60A
AGR2-C81S
D
HBEC
HBEC-AGR2-WT
Cell growth (Number of cell x10^6/cm^2)
Days after seeding
***
E
HBEC-AGR2-WT
HBEC-AGR2-E60A
ns
F
HBEC-AGR2-WT
HBEC-AGR2-C81S
ns

Figure 2

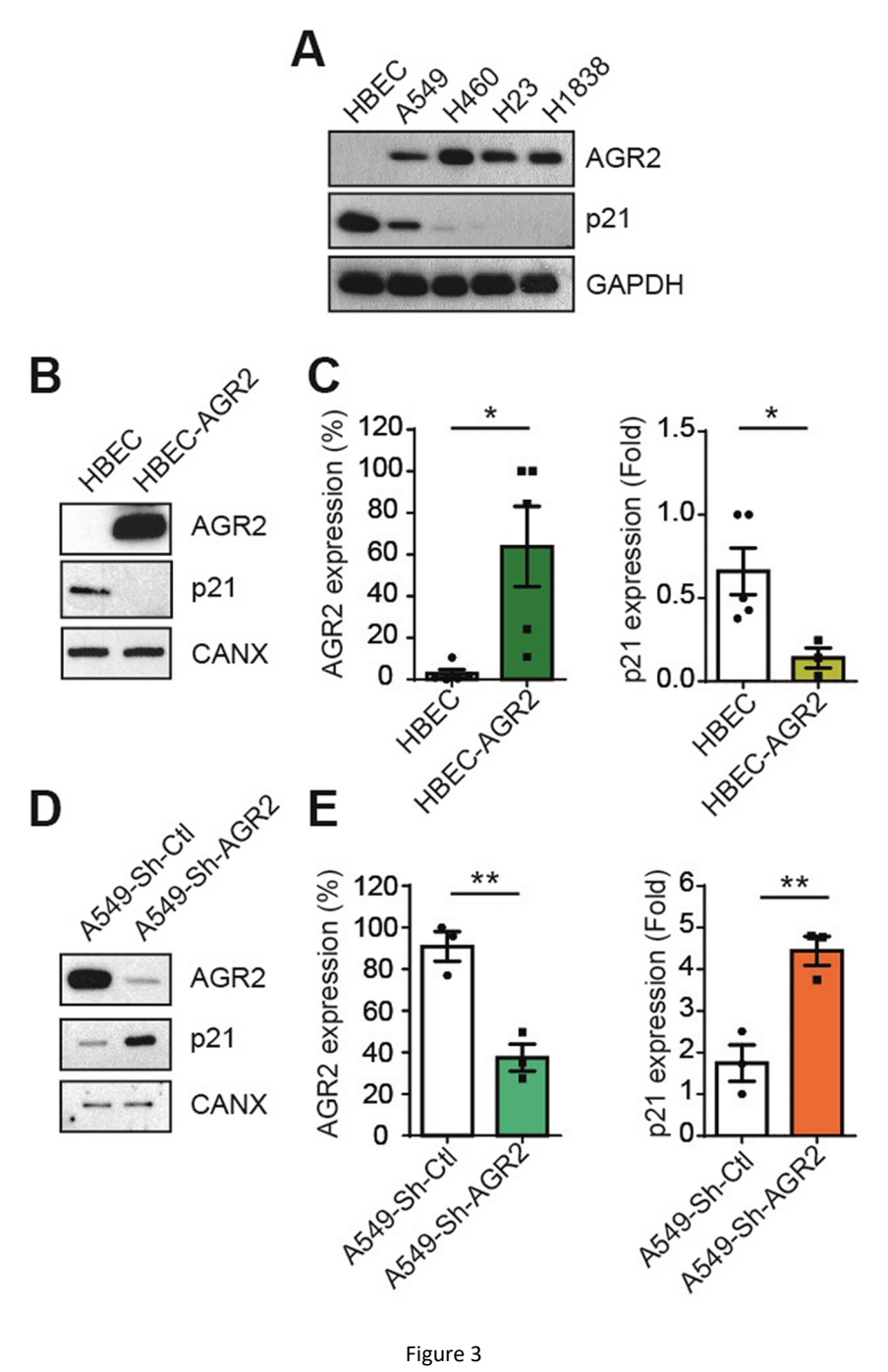
A
HBEC
A549
H460
H23
H1838
AGR2
p21
GAPDH
B
HBEC
HBEC-AGR2
AGR2
p21
CANX
C
AGR2 expression (%)
120
100
80
60
40
20
0
*
HBEC
HBEC-AGR2
p21 expression (Fold)
1.5
1.0
0.5
0.0
*
HBEC
HBEC-AGR2
D
A549-Sh-Ctl
A549-Sh-AGR2
AGR2
p21
CANX
E
AGR2 expression (%)
120
100
80
60
40
20
0
**
A549-Sh-Ctl
A549-Sh-AGR2
p21 expression (Fold)
6
5
4
3
2
1
0
**
A549-Sh-Ctl
A549-Sh-AGR2

Figure 3

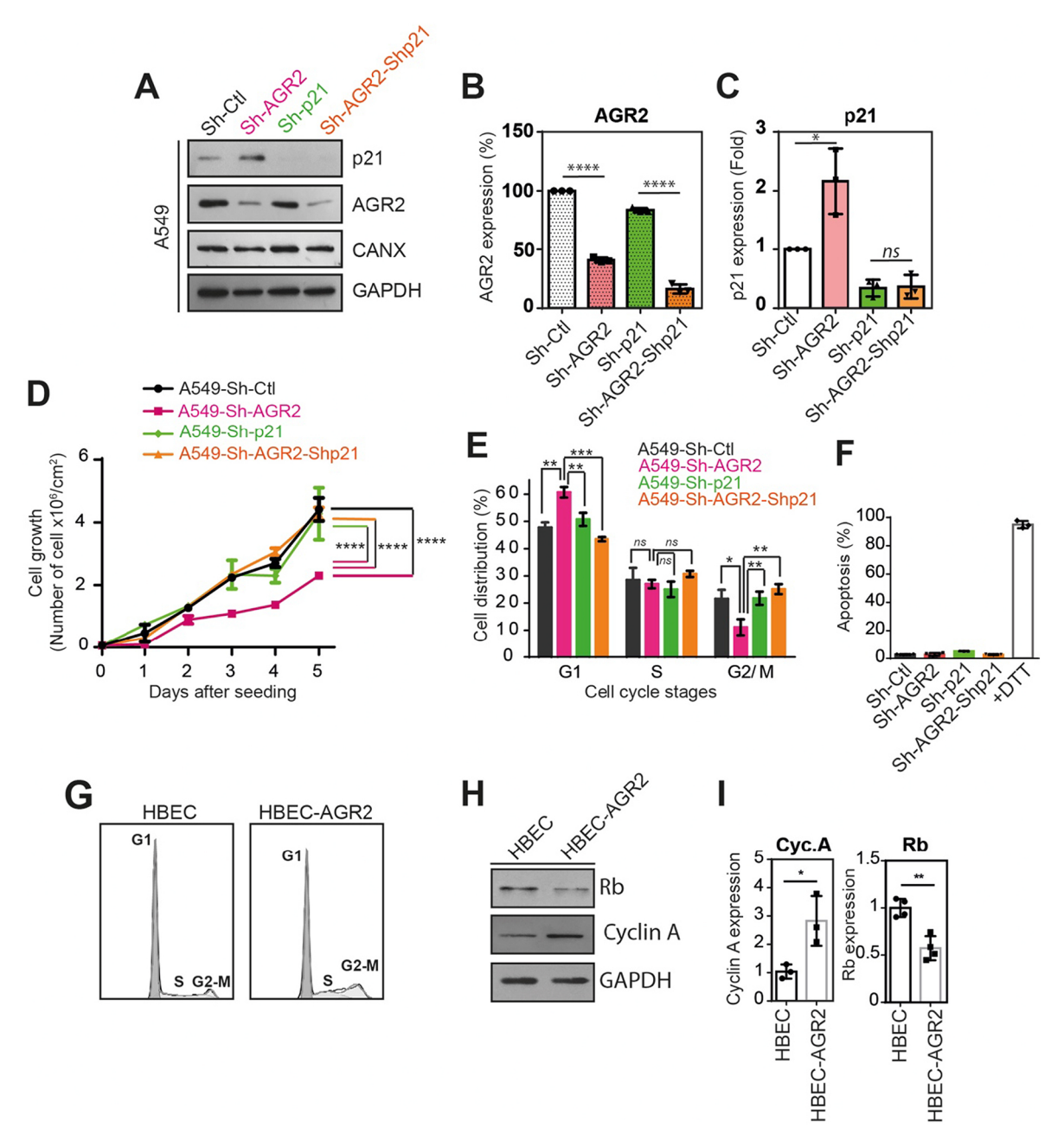
A
Sh-Ctl
Sh-AGR2
Sh-p21
Sh-AGR2-Shp21
A549
p21
AGR2
CANX
GAPDH
B
AGR2
AGR2 expression (%)
150
100
50
0
****
****
Sh-Ctl
Sh-AGR2
Sh-p21
Sh-AGR2-Shp21
C
p21
p21 expression (Fold)
3
2
1
0
*
ns
Sh-Ctl
Sh-AGR2
Sh-p21
Sh-AGR2-Shp21
D
A549-Sh-Ctl
A549-Sh-AGR2
A549-Sh-p21
A549-Sh-AGR2-Shp21
Cell growth
(Number of cell x10⁶/cm²)
6
4
2
0
0 1 2 3 4 5
Days after seeding
****
****
****
E
A549-Sh-Ctl
A549-Sh-AGR2
A549-Sh-p21
A549-Sh-AGR2-Shp21
Cell distribution (%)
60
50
40
30
20
10
0
**
***
**
ns
ns
ns
*
**
**
G1
S
G2/ M
Cell cycle stages
F
Apoptosis (%)
100
80
60
40
20
0
Sh-Ctl
Sh-AGR2
Sh-p21
Sh-AGR2-Shp21
+DTT
G
HBEC
HBEC-AGR2
G1
S
G2-M
G1
S
G2-M
H
HBEC
HBEC-AGR2
Rb
Cyclin A
GAPDH
I
Cyc.A
Cyclin A expression
5
4
3
2
1
0
*
HBEC
HBEC-AGR2
Rb
Rb expression
1.5
1
0.5
0
**
HBEC
HBEC-AGR2

Figure 4

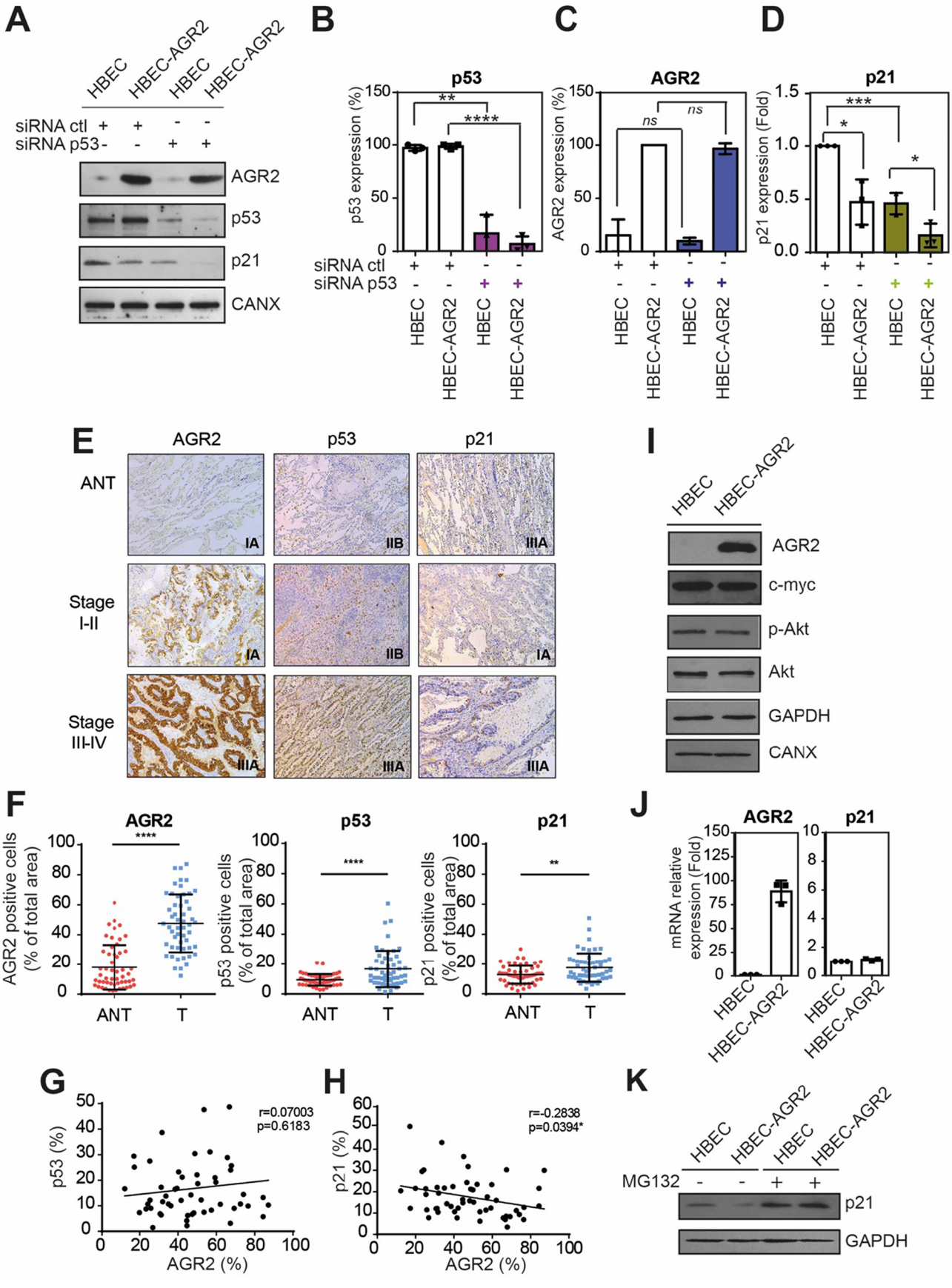
A
HBEC
HBEC-AGR2
HBEC
HBEC-AGR2
siRNA ctl + + - -
siRNA p53 - - + +
AGR2
p53
p21
CANX
B
p53
p53 expression (%)
150
100
50
0
**
****
siRNA ctl + + - -
siRNA p53 - - + +
HBEC
HBEC-AGR2
HBEC
HBEC-AGR2
C
AGR2
AGR2 expression (%)
150
100
50
0
ns
ns
HBEC
HBEC-AGR2
HBEC
HBEC-AGR2
D
p21
p21 expression (Fold)
1.5
1.0
0.5
0.0
***
*
*
HBEC
HBEC-AGR2
HBEC
HBEC-AGR2
E
AGR2
p53
p21
ANT
IA
IIB
IIIA
Stage I-II
IA
IIB
IA
Stage III-IV
IIIA
IIIA
IIIA
I
HBEC
HBEC-AGR2
AGR2
c-myc
p-Akt
Akt
GAPDH
CANX
F
AGR2
AGR2 positive cells (% of total area)
100
80
60
40
20
0
****
ANT
T
p53
p53 positive cells (% of total area)
100
80
60
40
20
0
****
ANT
T
p21
p21 positive cells (% of total area)
100
80
60
40
20
0
**
ANT
T
J
AGR2
mRNA relative expression (Fold)
150
125
100
75
50
25
0
HBEC
HBEC-AGR2
p21
10
8
6
4
2
0
HBEC
HBEC-AGR2
G
p53 (%)
50
40
30
20
10
0
r=0.07003
p=0.6183
0
20
40
60
80
100
AGR2 (%)
H
p21 (%)
60
50
40
30
20
10
0
r=-0.2838
p=0.0394*
0
20
40
60
80
100
AGR2 (%)
K
HBEC
HBEC-AGR2
HBEC
HBEC-AGR2
MG132 - - + +
p21
GAPDH

Figure 5

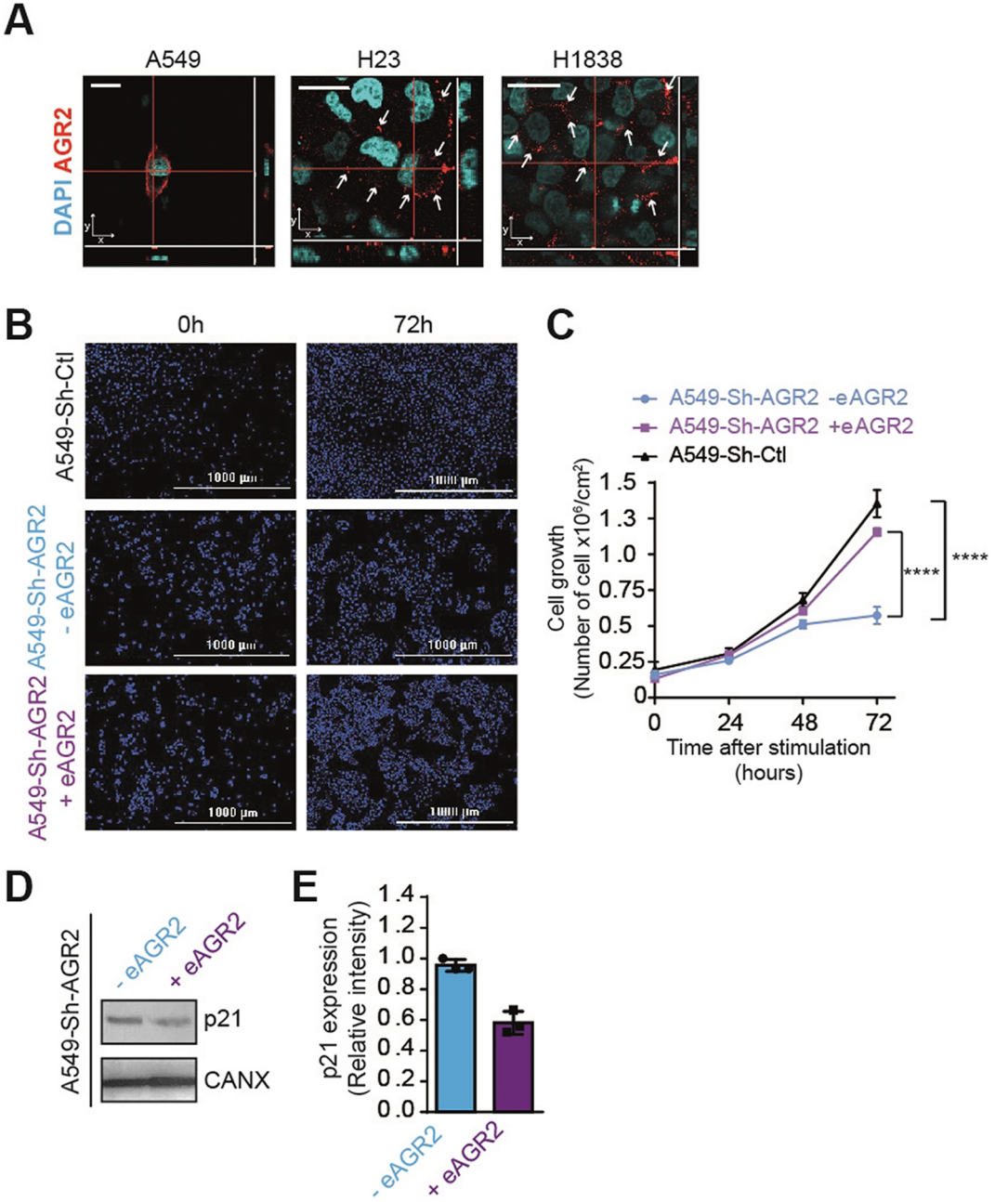
A
A549
H23
H1838
DAPI AGR2
B
0h
72h
A549-Sh-Ctl
A549-Sh-AGR2 - eAGR2
A549-Sh-AGR2 + eAGR2
1000 µm
C
A549-Sh-AGR2 -eAGR2
A549-Sh-AGR2 +eAGR2
A549-Sh-Ctl
Cell growth (Number of cell x10⁶/cm²)
1.5
1.3
1.0
0.75
0.5
0.25
0
0
24
48
72
Time after stimulation (hours)
****
****
D
A549-Sh-AGR2
- eAGR2
+ eAGR2
p21
CANX
E
p21 expression (Relative intensity)
1.4
1.2
1.0
0.8
0.6
0.4
0.2
0.0
- eAGR2
+ eAGR2

Figure 6

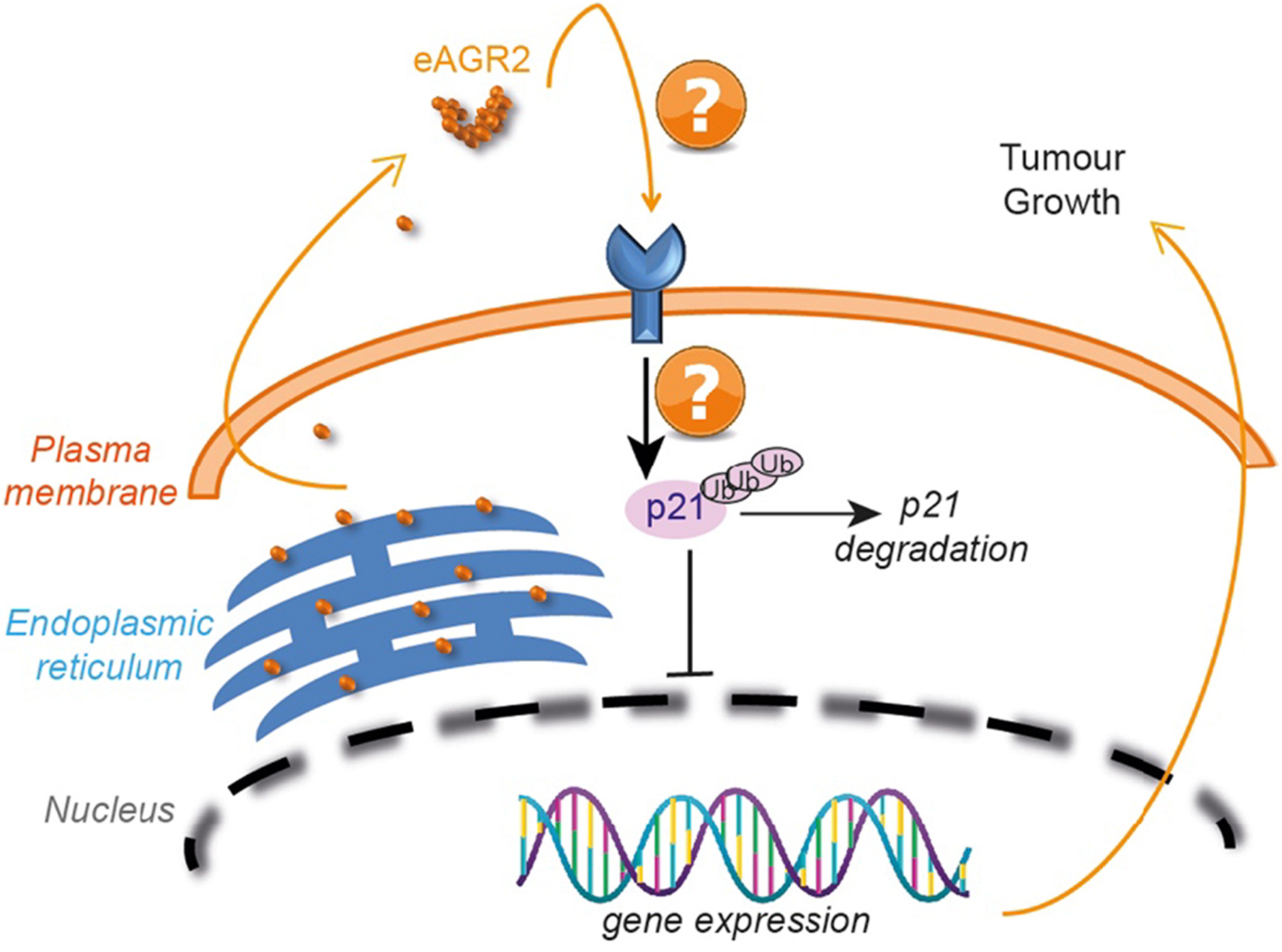
eAGR2
?
Tumour
Growth
?
Plasma
membrane
Ub
Ub
Ub
p21
p21
degradation
Endoplasmic
reticulum
Nucleus
gene expression

Figure 7